BNL-225380-2024-JAAM

An investigation on the structural stability of ZIF-8 in water versus water-derived oxidative species in aqueous environment

N. Talukder, X. Tong

To be published in "Microporous and Mesoporous Materials"

February 2024

Center for Functional Nanomaterials

Brookhaven National Laboratory

U.S. Department of Energy

USDOE Office of Science (SC), Basic Energy Sciences (BES). Scientific User Facilities (SUF)

DISCLAIMER

Title:

An Investigation on the Structural Stability of ZIF-8 in Water versus Water-derived Oxidative Species in Aqueous Environment

Niladri Talukder[a], Yudong Wang[a], Bharath Babu Nunna[b,c,d], Xiao Tong[e], Eon Soo Lee[a*]

[a] Advanced Energy Systems and Microdevices Laboratory, Department of Mechanical and Industrial Engineering, New Jersey Institute of Technology, Newark, NJ, 07102, USA.

[b] Department of Mechanical Engineering, Weber State University, Ogden, Utah, 84408, USA.

[c] Division of Engineering in Medicine, Department of Medicine, Brigham and Women's Hospital, Harvard Medical School, Harvard University, Cambridge, MA 02139, USA

[d] Harvard Graduate School of Education, Harvard University, Cambridge, MA 02138, USA.

[e] The Center for Functional Nanomaterials, Brookhaven National Laboratory, Upton, New York 11973, USA.

*** Corresponding author:**

Eon Soo Lee, Ph.D

Associate Professor,
Department of Mechanical and Industrial Engineering,
New Jersey Institute of Technology,
200 Central Avenue, Rm MEC 313
Newark, NJ07102-1982
973-596-3318 Office
eonsoo.lee@njit.edu
ORCID ID: 0000-0001-5863-3108

Abstract:

The zeolitic-imidazolate-framework-8 (ZIF-8) is one of the extensively studied metal-organic frameworks (MOF) materials because of its unique structure. For its potential applicability in numerous fields, it becomes crucial to have detailed studies on the structural stability of ZIF-8, especially in aqueous environments. A number of studies have been conducted to investigate the breakdown process of the ZIF-8 structure in water; which is known as the hydrolysis of ZIF-8. However, those studies reported different opposing experimental observations on the role of water on the structural stability of ZIF-8, which created obscurity in understanding this phenomenon. This study explored the effects of different water-derived species on the structural stability of ZIF-8; specifically, examined the effects of only water and water with different oxidative species that may be generated by water molecules' dissociation under external energy or catalyst presence. To this effort, we experimentally probed the physical and chemical structural changes of ZIF-8 in DI water and three different solutions of hydrogen peroxides (H_2O_2); taking H_2O_2 as the source of oxidative species. To assess the changes in elemental compositions, chemical bonds, functional groups, crystal structure, and morphology, all the samples were analyzed by X-ray photoelectron spectroscopy (XPS), energy-dispersive x-ray (EDX) spectroscopy, Fourier Transform Infrared (FTIR) spectroscope, X-ray diffractometer (XRD), and scanning electron microscope (SEM). Significant structural changes in ZIF-8 occurred mainly in the presence of oxidative species in water. Notably, oxidative species' concentration exceeding 1 M heightened the deformation of the ZIF-8 structure.

Keywords: Zeolitic-imidazolate-framework-8 (ZIF-8), ZIF-8 stability; ZIF-8 hydrolysis; Effect of oxidative species on ZIF-8; ZIF-8 crystal structure.

1. Introduction:

Metal-organic frameworks (MOFs) are a class of material where different framework structures are formed by a variety of orientations of transition metal atoms (Zn, Cu, Co, Fe, etc.) and their organic linkers [1–5]. Such structural coordination induces different properties in the material such as high porosity, extended surface area, various electrochemically active sites, etc. which are appealing for versatile applications such as CO_2 capturing [6–8], hydrogen storage [9–11], natural gas storage [12,13], water purification [14,15] catalysis [16–19], magnetism [20,21], chemical and biosensing [22] biomedical applications [23–26], and so on. Zeolitic imidazolate frameworks (ZIFs) are a specific type of MOF where the framework structures resemble the microporous crystal structure of zeolites. Zeolitic imidazolate framework-8 (ZIF-8) is the most familiar of the ZIF materials. In ZIF-8, the tetrahedrally coordinated zinc atoms bond with the

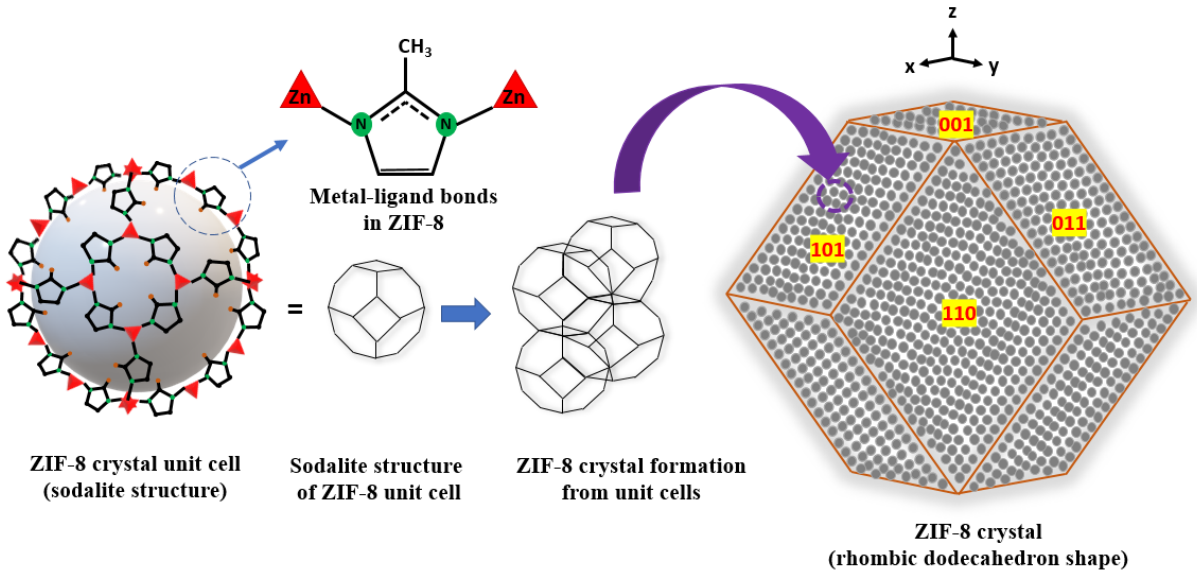

Figure 1: Schematics of ZIF-8 crystal unit cell; sodalite shape of the unit cell; formation of ZIF-8 crystal from unit cells; and ZIF-8 crystal with planes denoted with miller indices from an arbitrary reference coordinate. Schematics are not in actual size scales.

nitrogen sites of organic linkers 2-methylimidazole (HMIM) and form unit cells of sodalite structure; unit cell side length is around 16.99 Å [27]. These unit cells coordinate among themselves to form truncated rhombic dodecahedron or rhombic dodecahedron crystal structures. Figure 1 presents the chemical structural form of the ZIF-8's unit cell and its crystal structures. Such unique structural characteristics of ZIF-8 hint at its applicability in diversified areas; hence, numerous research communities have invested focus on the material.

Numerous studies reported the application of ZIF-8 as a carbon dioxide (CO_2) absorber, hydrogen and natural gas storage, photocatalysts, electrochemical catalysts, water-purifying materials, biomedical materials, etc. [28–36]. Many such applications require the material to operate in different aqueous environments. Hence, investigating the material's stability in different water-based environments became a concern [37]. A number of studies have been conducted on the structural and chemical stability of ZIF-8 in water-based environments. However, the stability of ZIF-8 in water remained largely debated to this date. Compiling experimental studies have been reported in recent years showing both the structurally stable and unstable nature of ZIF-8 in the aqueous medium. The disintegration of the ZIF-8 structure in contact with water is known as ZIF-8 hydrolysis in literature.

Different experimental observations suggested high structural stability of ZIF-8 in water. In a study by Park et al. [38], ZIF-8 powder was suspended in boiling water for 1-7 days. The powder x-ray diffraction (PXRD) patterns of the sample indicated no crystal structural changes of the material over the test period. Sheng et al. [39] reported that the water stability of ZIF-8 has a dependency on the type of zinc salts used in the synthesis process of the material. ZIF-8 produced from zinc acetate salt exhibited much higher hydrothermal stability than the ZIF-8 produced with zinc nitrate salt which is most commonly used. They suspended four ZIF-8

samples (synthesized with four different zinc salts) in water at 80 °C for up to ten days. While all of the samples maintained structural stability for seven days in terms of morphological and crystal structure, the ZIF-8 sample produced with zinc acetate could maintain its structural stability for full ten days. No further details were provided in this study to understand why the same material synthesized from different zinc salts showed different stability in water. More recently, while investigating the applicability of ZIF-8 as a means of drug delivery, Ahmed et al. reported through absorption-based experiments that ZIF-8 samples maintained a high thermal and aqueous stability [25]. Li et al. and Jiang et al. investigated the applicability of ZIF-8 for the removal of arsenate and benzotriazoles respectively from aqueous environments [14,15]. From their experiments, it was seen that ZIF-8 did not lose its adsorption capacity for a considerable time frame and the material was also reusable.

Contrary to the above-mentioned reports, different studies implicated the vulnerability of ZIF-8 structure in aqueous environments. Taheri et al. reported that the ZIF-8 structure decomposes in the presence of water to some degree, however, the process is accelerated in the presence of UV light [40]. In multiple accounts, Zhang et al. reported the hydrolysis of ZIF-8 occurring in elevated temperatures as well as ambient conditions [41–43]. They also reported that when the hydrolyzed ZIF-8 is condensed back to the solid state by evaporating water, a new substance with an almost identical composition as ZIF-8 is formed but with an altered crystalline structure. Tanaka et al. presented that the pristine ZIF-8 could maintain its structural form after being immersed and stirred in water at room temperature for seven days [44]. However, as the same experiments were performed at an elevated temperature of 90° C, the sample structurally decomposed to a degree. They also reported that when the outermost layer of ZIF-8 can be made carbon-rich, the material exhibits higher hydrothermal stability and absorptivity.

From the above-mentioned group of studies we can note some postulations on the hydrothermal stability of ZIF-8: the type of precursor materials and synthesis process may have an effect on the water stability of ZIF-8; the experimental conditions to examine the material's stability in water such as experiment time, ZIF-8 to water ratio, supplied external energy, etc. may have influences on the structural stability of ZIF-8 in the aqueous environment; doping of integrations of other materials also influences the hydrothermal stability of ZIF-8; the stability of ZIF-8 in aqueous medium may be tuned by functionalizing the imidazolate linker with different anions.

Asides from reaching any conclusions on the ZIF-8 hydrolysis process these postulations generate further intriguing questions on the key influencing factors of this process. Nonetheless, the most anticipated path of the ZIF-8 hydrolysis process was reported as the breakdown of Zn-N (metal-ligand) bonds, and the formation of Zn-OH moieties or ZnO species in contact with water [41]. However, only a very few studies are found that focused on this process. Besides, seemingly no compiling reports were found to probe whether the water molecules alone could break off the Zn-N bonds without being assisted by externally supplied energy to the test environments. Nonetheless, the studies on ZIF-8 hydrolysis provide an indication that in the test environments, different oxidative species may be formed upon the dissociation of water molecules in presence of externally supplied energy, impurities remained from the ZIF-8 synthesis process, and different electronically active parts of the ZIF-8 structure [39,40]. These species may intensify the Zn-N bond breakdown process. Furthermore, in different practical applications of ZIF-8-based materials, especially in electrochemical environments, the presence of different oxidative species is obvious. It is therefore essential to investigate the ZIF-8 hydrolysis process from this perspective of the presence of oxidative species in the aqueous test environment to achieve a clearer perception.

In this study, we attempted to understand the ZIF-8 hydrolysis process from the perspective of the presence of different oxidative species in the aqueous test environment. To this effort, we have treated ZIF-8 with DI water and aqueous solutions of hydrogen peroxide (H_2O_2) of three different concentrations as H_2O_2 can be readily decomposed in water and produce a variety of oxidative species and radicles such as HO-, OH•, H•, and OOH• [45,46]. The treated ZIF-8 samples were examined for elemental composition changes, chemical bond changes, functional group changes, crystal structure changes, and morphological changes. The experimental findings of this study should aid concerned research communities to gain a clearer view of the ZIF-8 hydrolysis process.

2. Materials and Methods:

2.1 Sample preparation:

ZIF-8 was purchased from Aldrich (Basolite Z1200) which is a white powder; used as the base sample; the rest of the samples were compared with it for structural and chemical properties. For the hydrolysis investigation, first, 80 mg of ZIF-8 powder was mixed with 1 ml of deionized water. The mixture in the sealed container was subjected to vortex mixing for two hours at room temperature so that the effect of water on the structural changes of ZIF-8 can be observed. Then the mixture was dried out and the water treated ZIF-8 samples were collected in powder form. In a similar manner 80 mg of ZIF-8 was mixed with (1 ml each) three different concentrations of H_2O_2 solutions 0.01 M, 0.1 M, and 1 M and subjected to vortex mixing During the vortex mixing process of ZIF-8 and H_2O_2 mixtures color changes were noticed, apparent the mixtures reacted exothermically; at a much higher rate for ZIF-8 and 1 M H_2O_2 container forming gas bubbles.

After two hours of mixing, the samples were dried out in a vacuum chamber (in ~ -50 kPa) to remove any possible guest molecules in the pores of ZIF-8, then the samples were collected for characterization. As it was intended to examine only the effects of water and hydrogen peroxide solutions on the structure of ZIF-8, the samples were not subjected to any further thermal or chemical process after the water and H_2O_2 treatment step. A 5 M H_2O_2 ZIF-8 sample preparation was also attempted, however, the reactivity was too high and exothermic for that mixture, so it was discarded.

2.2 Elemental composition and chemical bonds and functional group evaluation method:

The chemical structural changes of the ZIF-8 samples in terms of elemental compositions and relative ratios of different major elements C, N, and Zn were evaluated by x-ray photoelectron spectroscopy (XPS) survey scan spectra analysis and element-specific narrow scan spectra analysis through fitting peaks on them for different chemical bonds. The XPS investigations were carried out in an ultrahigh vacuum (UHV) system with base pressures below 5x10-9 Torr. The system is equipped with a twin anode X-ray source (SPECS, XR50). Al Kα (1486.7 eV) radiation was used at 10 kV and 30 mA and a hemispherical electron energy analyzer (SPECS, PHOIBOS 100). The angle between the analyzer and X-ray source is 45° and photoelectrons were collected from the sample surface perpendicularly. The adventitious carbon located at 284.5 eV was used to calibrate the XPS peak positions. XPS data were analyzed using Casa XPS.

Taking into account that XPS is primarily a method for characterizing surfaces, probing only a few nanometers beneath the material's surface, the elemental composition of ZIF-8's bulk was additionally determined through energy-dispersive x-ray (EDX) spectroscopy. This was carried

out using a JEOL JSM-7600F scanning electron microscope (SEM) equipped with an EDS analyzer.

In order to further validate the major chemical changes identified in the ZIF-8's chemical structure as indicated by the XPS analysis due to the influence of water and H_2O_2, the samples were further analyzed using a Fourier Transform Infrared (FTIR) spectroscope (Nicolet 6700 FT-IR spectrometer); especially to detect the changes in the chemical functional groups on the ZIF-8 structure due to water and H_2O_2 treatments.

2.3 Crystal structure evaluation method:

The ZIF-8 samples were analyzed by an EMPYREAN, Philips multipurpose X-Ray Diffractometer (XRD) system to determine the changes in the crystal structures caused by water and H_2O_2 treatments. To avoid data noise the samples were mounted on the XRD system by placing them on a zero-background detraction holder of pure silicon (9N). The diffraction peaks of ZIF-8 samples were analyzed with reference to the ZIF-8 diffraction data from International Centre for Diffraction Data (ICDD).

2.4 Morphological evaluation method:

To evaluate the changes in morphology from the pure ZIF-8 to water-treated ZIF-8 to H_2O_2-treated ZIF-8 samples SEM imaging was employed to observe the material structures up to 100 nm scale. The submicron scale SEM images were obtained by a JEOL JSM-7600F SEM system.

3. Results and Discussion:

3.1 Elemental composition changes:

Table 1: Surface elemental composition of ZIF-8, DI water treated ZIF-8, and 0.1, 0.1, and 1 M H_2O_2 treated ZIF-8 samples; obtained by UHV-XPS survey scan.

Samples	Nitrogen (N) relative atomic ratio	Zinc (Zn) relative atomic ratio	Carbon (C) relative atomic ratio	Oxygen (O) relative atomic ratio
	(%)	(%)	(%)	(%)
ZIF-8	25.87 ± 0.85	3.45 ± 0.09	62.94 ± 1.35	7.74 ± 0.58
ZIF-8 + H_2O (Water)	24.59 ± 0.50	3.23 ± 0.19	63.69 ± 0.82	8.49 ± 0.40
ZIF-8 + 0.01 M H_2O_2	25.76 ± 0.31	3.12 ± 0.28	64.95 ± 0.85	6.17 ± 0.94
ZIF-8 + 0.1 M H_2O_2	26.64 ± 1.95	3.19 ± 0.09	64.01 ± 0.53	6.16 ± 1.96
ZIF-8 + 1 M H_2O_2	24.91 ± 0.38	2.84 ± 0.09	55.34 ± 2.27	16.91 ± 2.11

To determine the changes in the relative elemental ratios of the major elements on the ZIF-8 samples' surfaces due to the effect of water and H_2O_2 solutions, three sets of pure ZIF-8, water-treated, and H_2O_2-treated ZIF-8 samples were analyzed by UHV-XPS. A set of XPS survey measurements spectra are provided in the supplementary file (Figures S-1 to S-5). Table 1 presents the averaged (with a standard deviation) relative elemental ratios of nitrogen, zinc, carbon, and oxygen of the samples obtained by the XPS survey scan. The data appeared to be consistent with previously reports [47,48]. The possible source of the oxygen content in the pure ZIF-8 sample are physorbed/particulate oxygen appeared during the sample preparation process for XPS analysis [15,41,44]. It's important to highlight that the XPS analysis often faces issues with surface oxygen content. Additionally, because XPS (as well as EDX) cannot identify

hydrogen (H) atoms, the relative elemental ratio of ZIF-8 may deviate from what is calculated based on the standard chemical formula of ZIF-8 ($Zn(MIM)_2$ or $C_8H_{12}N_4Zn$). Nevertheless, it is reasonable to assume that since all ZIF-8 samples (both untreated and treated) encountered the same experimental issues, the effects of water and H_2O_2 treatments on ZIF-8 can still be reasonably discerned from these data. The elemental ratios of the pure ZIF-8 and water-treated ZIF-8 appeared similar indicating that the material's elemental composition did not change considerably in contact with water for two hours. A drop in the oxygen content was observed in the 0.01 M H_2O_2-treated ZIF-8 sample indicating that the species from H_2O_2 may have removed the oxygen contents from the ZIF-8 surface at the treatment condition. The ratio of zinc slightly declined to indicate the removal of zinc atoms from the material surface on a smaller scale most like in the form of zinc oxide [41]. An increase in the carbon contents also suggests the removal of oxygen species from the ZIF-8 surface. Treatment with 0.1 M H_2O_2 also indicate the removal of the oxygen contents from the ZIF-8 surface and no other significant changes were observed. In the 1 M H_2O_2-treated ZIF-8, a dramatic increase in the oxygen contents was observed; raised approximately little more than two times from ~ 7.74% to 16.91%. This indicates that at this treatment condition, the species from H_2O_2 may have reacted with different parts of ZIF-8 and originated the material surface. The reduction of carbon, nitrogen, and zinc contents of ZIF-8 at this condition also indicates that a layer of oxygen-containing species formed on the material's surface. However, considering the margin of error, these data can not conclusively suggest significant chemical alterations in the ZIF-8 structure. Hence, additional analysis of these samples through XPS narrow scans and FTIR spectroscopy is discussed in subsequent sections.

To assess the bulk elemental composition changes in the ZIF-8 samples, relative elemental ratios were obtained by EDX analysis as presented in Table 2; measured at least three times for each

sample. A set of original EDX measurements data are provided in the supplementary file (Figures S-1 to S-5).

Table 2: Bulk elemental composition of ZIF-8, DI water treated ZIF-8, and 0.1, 0.1, and 1 M H_2O_2 treated ZIF-8 samples; obtained by EDX measurements.

Samples	Nitrogen (N) relative atomic ratio	Zinc (Zn) relative atomic ratio	Carbon (C) relative atomic ratio	Oxygen (O) relative atomic ratio
	(%)	(%)	(%)	(%)
ZIF-8	29.37 ± 4.06	7.51 ± 1.08	61.88 ± 3.10	1.24 ± 0.41
ZIF-8 + H_2O (Water)	27.86 ± 2.62	6.32 ± 1.24	64.54 ± 3.43	1.28 ± 0.68
ZIF-8 + 0.01 M H_2O_2	24.76 ± 1.67	10.27 ± 2.38	63.74 ± 1.06	1.40 ± 0.50
ZIF-8 + 0.1 M H_2O_2	30.87 ± 1.72	5.47 ± 0.76	62.30 ± 2.12	1.35 ± 0.48
ZIF-8 + 1 M H_2O_2	29.87 ± 0.84	7.07 ± 0.87	58.22 ± 0.37	4.85 ± 0.07

The relative elemental ratio of major elements (N, Zn, C) in the pure ZIF-8 sample, as determined by EDX, closely aligns with the elemental ratio calculated from ZIF-8's standard chemical formula (N : Zn : C = ~ 30.7 : 7.7 : 61.53, excluding H atoms). However, EDX measurements notably differ from those obtained by XPS, particularly concerning the relative percentage of oxygen. This discrepancy arises because XPS primarily analyzes the elemental ratio at the material's surface, where a significant amount of physisorbed/particulate oxygen is present. In contrast, EDX probes the elemental ratio from the material's bulk, which helps normalize the impact of physisorbed/particulate oxygen of the ZIF-8's surface on the relative elemental composition data. However, these observations suggest that, in the pure ZIF-8 samples, a substantial portion of the oxygen content was concentrated on its surface especially

on the ones prepared for XPS analysis. The relative ratios of Zinc in the ZIF-8 samples, as measured by EDX, are considerably higher than those obtained through XPS measurement. Such difference between XPS and EDX data is due to two factors: (1) within the framework structure of ZIF-8, the Zn content is substantially lower than the C and N contents, and the Zn atoms are surrounded by C and N atoms, as well as O atoms, particularly at the material's surface. This lower Zn content and the specific structural arrangement of Zn atoms in ZIF-8 significantly attenuate the energy of emitted photoelectrons from Zn atoms during XPS analysis, resulting in a lower detection of the Zn content in the material by XPS compared to EDX. Such an effect is not significant for the C and N because of their relative abundance in ZIF-8. (2) Additionally, the decrease in the relative ratio of oxygen in the EDX measurement, in contrast to the XPS data (achieved by normalizing the counts of physisorbed/particulate oxygen on the material's surface), also contributes to an increase in the relative ratios of Zn.

However, changes in the relative elemental ratios observed through EDX due to the impact of water and H_2O_2 treatments mirrored the trends indicated by XPS measurements. Considering the standard deviation in the data, no definitive changes were observed between the pure ZIF-8 and water-treated ZIF-8 samples. Consistent with XPS findings, EDX measurements clearly showed that the relative elemental ratios of ZIF-8 underwent significant changes following 1 M H_2O_2 treatment, with a notable increase in the oxygen's relative ratio and a decrease in the carbon's relative ratio. EDS data revealed that the oxygen's relative ratio increased approximately fourfold from ~1.24% to 4.85%, while this increase was roughly twofold in XPS data. This suggests that the rise in oxygen content due to the 1 M H_2O_2 treatment not only affected the surface of ZIF-8 but also increased oxygen content in the material's bulk.

The alterations in elemental composition observed through both XPS and EDX measurements,

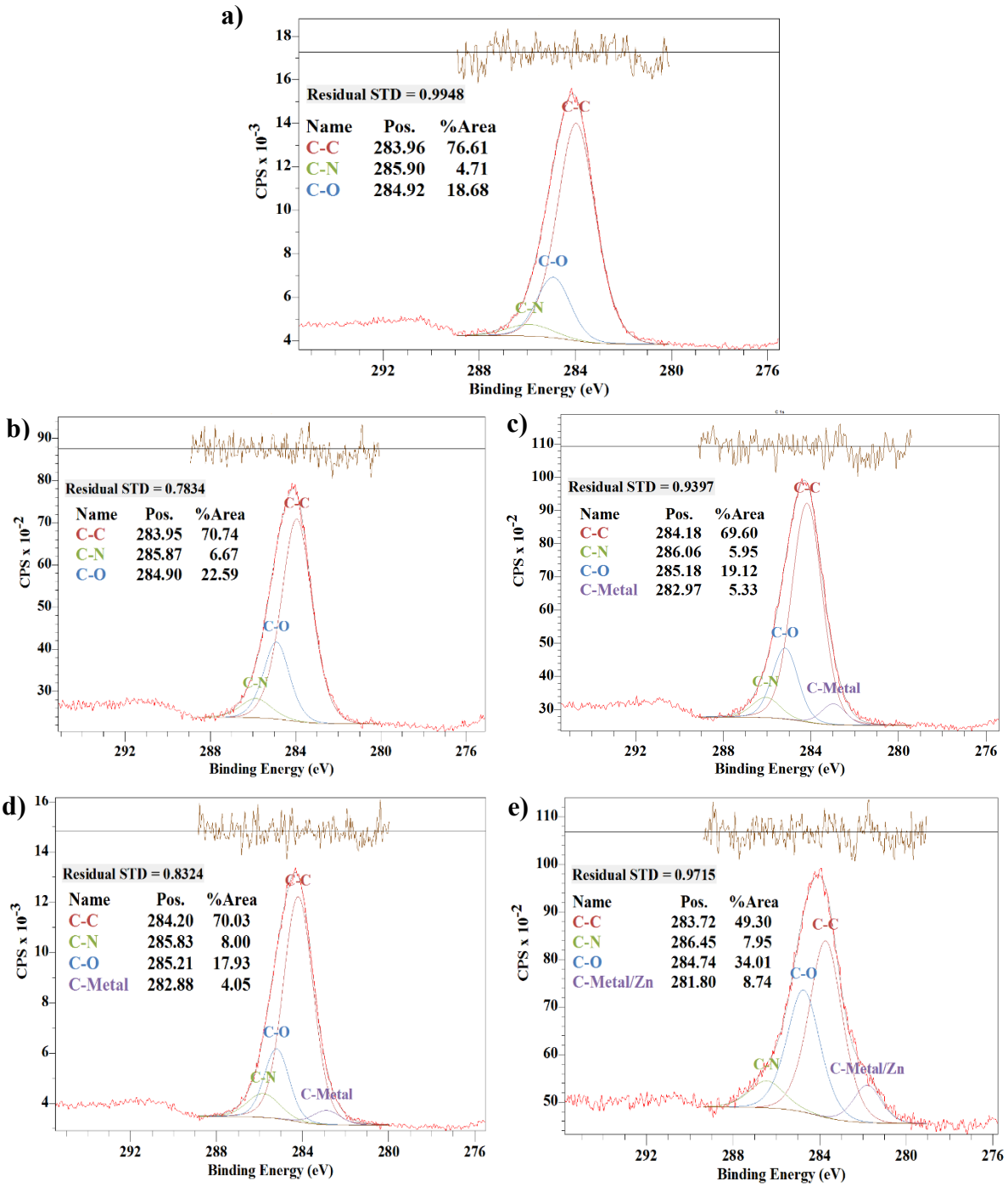

Figure 2: XPS C 1s narrow scan spectra of (a) ZIF-8; (b) DI water treated ZIF-8; (c-e) 0.01 M, 0.1 M, and 1 M H_2O_2 treated ZIF-8. The Data obtained from UHV-XPS experiments.

considering both the surface and bulk of the ZIF-8 samples, suggest that water treatment did not bring about significant changes in the material's composition. The most noticeable changes occurred with the 1 M H_2O_2 treatment.

3.2 Chemical bond changes:

To observe the changes in different chemical bonds of carbon, nitrogen, and zinc XPS narrow scans were obtained for C 1s, N 1s, and Zn 2p. Considering the relatively lower ratio of zinc and nitrogen, 30 scans were obtained consecutively to construct the Zn 2p and N 1s spectra. The relative ratios of the bonds were quantified by fitting peaks corresponding to the bonds. The Shirley background was used to construct the synthetic peaks. Peak fittings were completed by obtaining reasonable residual standard deviation between the experimental data curve and overall synthetic data envelop.

3.2.1 Changes in the Carbon bonds:

Figure 2 shows the C 1s narrow scan spectra of pure ZIF-8, water-treated ZIF-8, and three samples of H_2O_2-treated ZIF-8. To analyze the C 1s spectra by fitting peaks of major bonds of carbon in the material, the bonding energy of the C-C, C-N, C-O, and C-metal (carbides) bonds were considered 284-284.5 eV, 286 eV, 285 eV, and 282-283.5 eV respectively.

It is observed that the ratio of the C-C bond decreased by around 6% from the pure ZIF-8 sample to the water-treated ZIF-8 sample while the C-O bond ratio increased by around 4%. The ratio of C-N bonds was increased slightly. The C-C bonds in the ZIF-8 mainly represent the bond between the pentagonal ring of the imidazole and the methyl (-CH_3) group. The observed decline in the relative ratio of C-C bonds and the corresponding increase in the C-O and C-N bonds

indicate the probable dissociation of -CH_3 from the imidazolate ring of ZIF-8 structure and being replaced by oxygen-containing groups on a small scale; most possibly by the -OH group from water [26]. To verify such indication for the chemical changes, the samples were subjected to FTIR analysis, presented in a later section. The presence of the -CH_3 group in the ZIF-8 structure rationalizes the hydrophobic nature of the material and the water adsorption property of ZIF-8 can be tuned by linker functionalization with different anions [49]. Studies also showed that the nonpolar -CH_3 group can improve the MOF materials' stability and aqueous environments by shielding the material from the attack of aqueous species [50]. In this regard, it can be asserted that the replacement of -CH_3 of the ZIF-8 by polar groups such as -OH changes the hydrophobic nature of the ZIF-8 structure and makes it vulnerable to further structural deformation. The XPS C 1s data comparison of water-treated ZIF-8 with pure ZIF-8 sample suggests that the treatment of ZIF-8 with DI water for two hours at room temperature did not decrease the C-C bond ratio significantly, hence, did not significantly affect the structural stability of ZIF-8. This observation is supported by the crystal structural and morphological data presented in the later section.

However, in different previous studies, it was observed that the different ZIF-8 samples did go into structural deformation in water contact [26,41–43]. In this regard, it was also interesting to notice that in the ZIF-8 samples that were hydrolyzed even at room temperature, a considerable ratio -OH species were already present in the pristine form of those ZIF-8 samples which may have aided the hydrolysis process. Obviously, more specific studies are required to elucidate this issue which is beyond the scope of this current study.

Compared to the pure and water-treated sample, in the 0.01 M H_2O_2-treated ZIF-8 while the C-C and C-N bond ratio remained almost unchanged however the ratio of C-O bonds decreased slightly. This indicates that the oxygen contents were removed to a degree from the ZIF-8

surface; most likely by the H^+ ions from the H_2O_2 solution. A peak between 282-283.5 eV corresponding to the carbon-metal bond (C-metal) was observed for this sample suggesting the formation of bonds between carbon and zinc atoms. These observations suggest that the treatment of ZIF-8 with 0.01 M H_2O_2 solution did not affect the structural stability significantly. For the 0.1 M H_2O_2-treated sample, the ratio of C-O bonds further decreased slightly however no drastic changes were observed in the ratio of other carbon bonds.

In the 1 M H_2O_2-treated ZIF-8 sample, a dramatic decrease in the C-C bonds and an increase in the C-O bonds were observed which indicates a drastic change in the structure of the ZIF-8. The C-Zn bond ratio is found highest at the condition. In the pristine form of ZIF-8, it is expected that the Zn atoms form bonds with the N atoms of the imidazole linkers. The increase in the Zn-C bonds suggests the possible breakdown of Zn-N bonds which can lead to the destruction of the pristine form of the ZIF-8's unit cells. These observations together suggest that the oxidative species from 1 M H_2O_2 may have replaced the $-CH_3$ groups with -OH to a much higher degree. Also, the presence of polar -OH moiety in the ZIF-8 may have weakened the Zn-N bonds leading to their breakdown, ultimately causing a drastic alteration of the ZIF-8's structure. A clearer view on this indication may be found from the changes in the nitrogen and zinc bonds in the samples.

3.2.2 Changes in the Nitrogen bonds:

In the ZIF-8 structure, the nitrogen atoms prominently form bonds with zinc and carbon atoms. Especially the state of N-Zn bonds is purported to be one of the main indicators of the stability of the entire molecular and crystal structure of ZIF-8 in aqueous environments. To this aspect, it was essential to evaluate the changes in the nitrogen bonds of ZIF-8 due to water and H_2O_2

treatments in this study. The XPS N 1s narrow spectra of the ZIF-8 sample are presented in

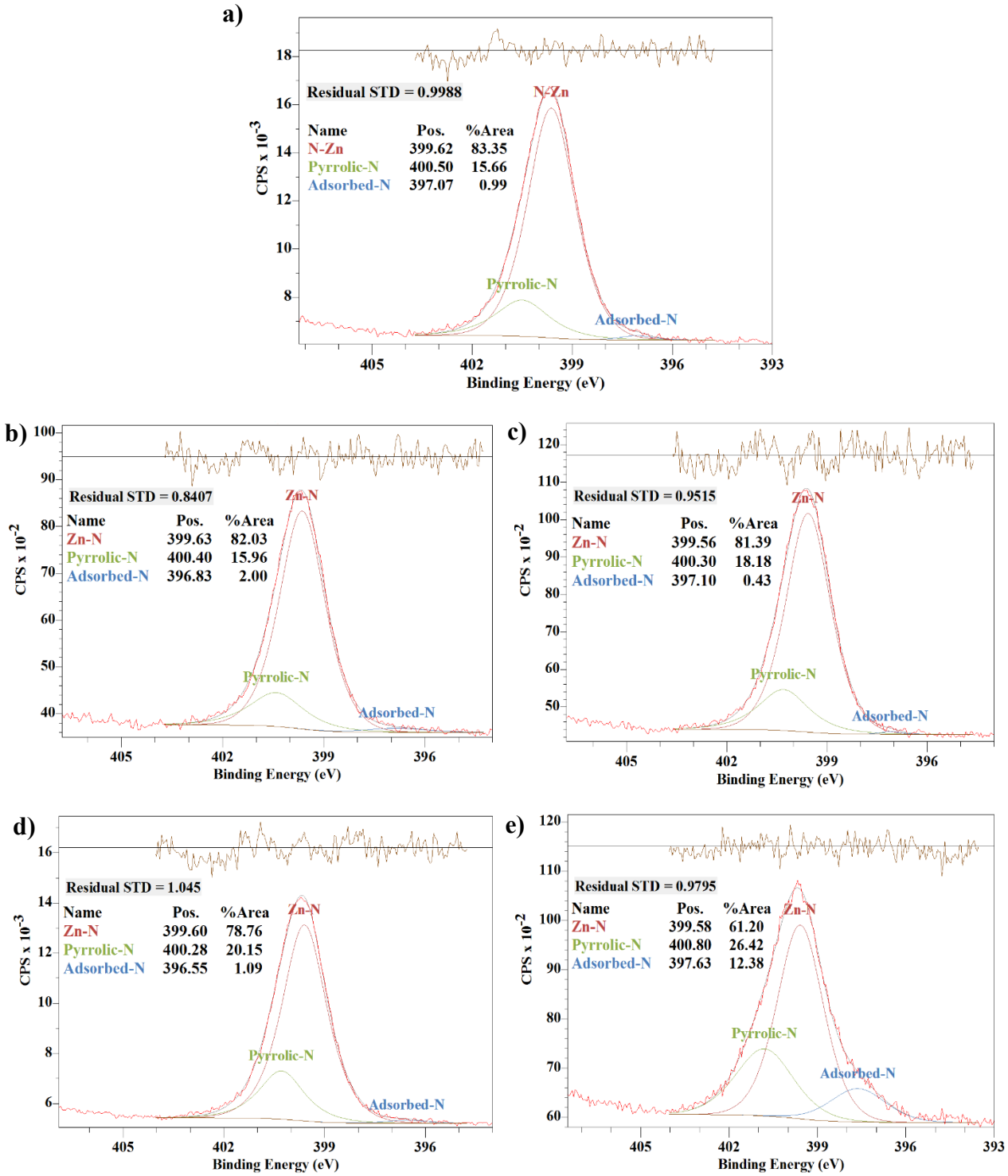

Figure 3: XPS N 1s narrow scan spectra of (a) ZIF-8; (b) DI water treated ZIF-8; (c-e) 0.01 M, 0.1 M, and 1 M H_2O_2 treated ZIF-8. The Data obtained from UHV-XPS experiments.

figure 3. Each of the N 1s spectra is fitted with three peaks corresponding to N-Zn, N-C (pyrrolic), and adsorbed-N on the surface of the material. The nitrogen atoms forming the pentagonal imidazole ring exhibit binding energy in the XPS analysis very close to the ones in the pyrrole ring, thus, for N-C bonds binding energy around 400.7 eV was considered. The peaks for N-Zn bonds correspond to around 399.4 eV [51,52]. The peaks correspond to adsorbed or particulate nitrogen with binding energies around 396.5 – 397.5 eV.

In the pure ZIF-8 sample, the N 1s spectrum is mainly composed of the N-Zn bonds followed by the N-C bonds. In the water-treated ZIF-8 sample, the nitrogen bonds were almost unchanged compared to the ones of pure ZIF-8. The N-Zn bonds were found to slightly decreased while the adsorbed nitrogen content increased slightly; which indicates that the water mildly affected the ZIF-8 structure. In the 0.01 M H_2O_2-treated ZIF-8, the N-Zn bond relative ratio slightly decreased further thus increasing the relative ratio of N-C bonds and the ratio of adsorbed nitrogen decreased compared to the water-treated ZIF-8 sample. These observations suggest that the ZIF-8 could maintain its structural integrity at this level of oxidative specie in the test environment. In the 0.1 M H_2O_2-treated ZIF-8 sample again the N-Zn bonds decreased slightly while the N-C bonds increased compared to the previous sample. However, these changes were not significant enough to conclude any drastic changes in the ZIF-8's structure at this test condition. The changes in the Zn-N and N-C bonds from pure ZIF-8 to 0.1M H_2O_2-treated ZIF-8 sample found by these XPS N 1s spectra analysis can not certainly suggest the structural changes of ZIF-8.

However, changes in the nitrogen bonds in the 1 M H_2O_2-treated ZIF-8 sample were obvious. The relative ratio of N-Zn bonds drastically dropped while a dramatic increase in the adsorbed nitrogen content was observed. This indicates a considerable change in the ZIF-8 structure by the

effect of 1 M H_2O_2-derived species. The XRD data and SEM image, presented in the later sections, also show a drastic change in the ZIF-8 structure for this sample. The oxidative species from 1 M H_2O_2 most likely started attacking N-Zn bonds at a much higher degree [41]; the nitrogen atoms remained on the material's surface in an adsorbed form. Besides, at this point, it is also reasonable to correlate the simultaneous dramatic increase in the C-O bond ratio, observed in the C 1s spectra analysis, and the considerable decrease in the N-Zn bond ratio in this sample. The degree of the breakdown of N-Zn bonds may be influenced by the degree of increase in the -OH group in the ZIF-8 structure. If the nonpolar -CH_3 moiety of ZIF-8 is replaced by the polar -OH group, it is obvious that a shift in the electronic structures of the adjacent C, N atoms will occur which may play a role in the weakening of the N-Zn bond [53,54]. Further targeted investigations may be conducted on this aspect which is beyond the scope of this study.

3.2.3 Changes in the Zinc bonds:

For complimentary confirmation of the changes in carbon and nitrogen bonds, Zn 2p narrow scan spectra of the ZIF-8 samples were obtain ed. Two peaks corresponding to Zn 2p 1/2 and Zn 2p 3/2 were observed at the bonding energy around 1045 eV and 1021 eV respectively. The Zn 2p 3/2 peak was fitted with Zn-N, Zn-O or Zn-OH, and Zn-C bonds correspond to the bonding energy around 1021.4 eV, 1022.1 eV, and 1019 eV respectively. The Zn 2p spectra are shown in figure 4.

For the pure ZIF-8 sample, the Zn 2p 3/2 is dominated by the Zn-N bonds. Also, the XPS data indicate the existence of Zn-O/Zn-OH and a trace amount of Zn-C bond in the material. The Zn-

N bonds are found to be in a slightly declining trend from pure ZIF-8 to water treated ZIF-8 to

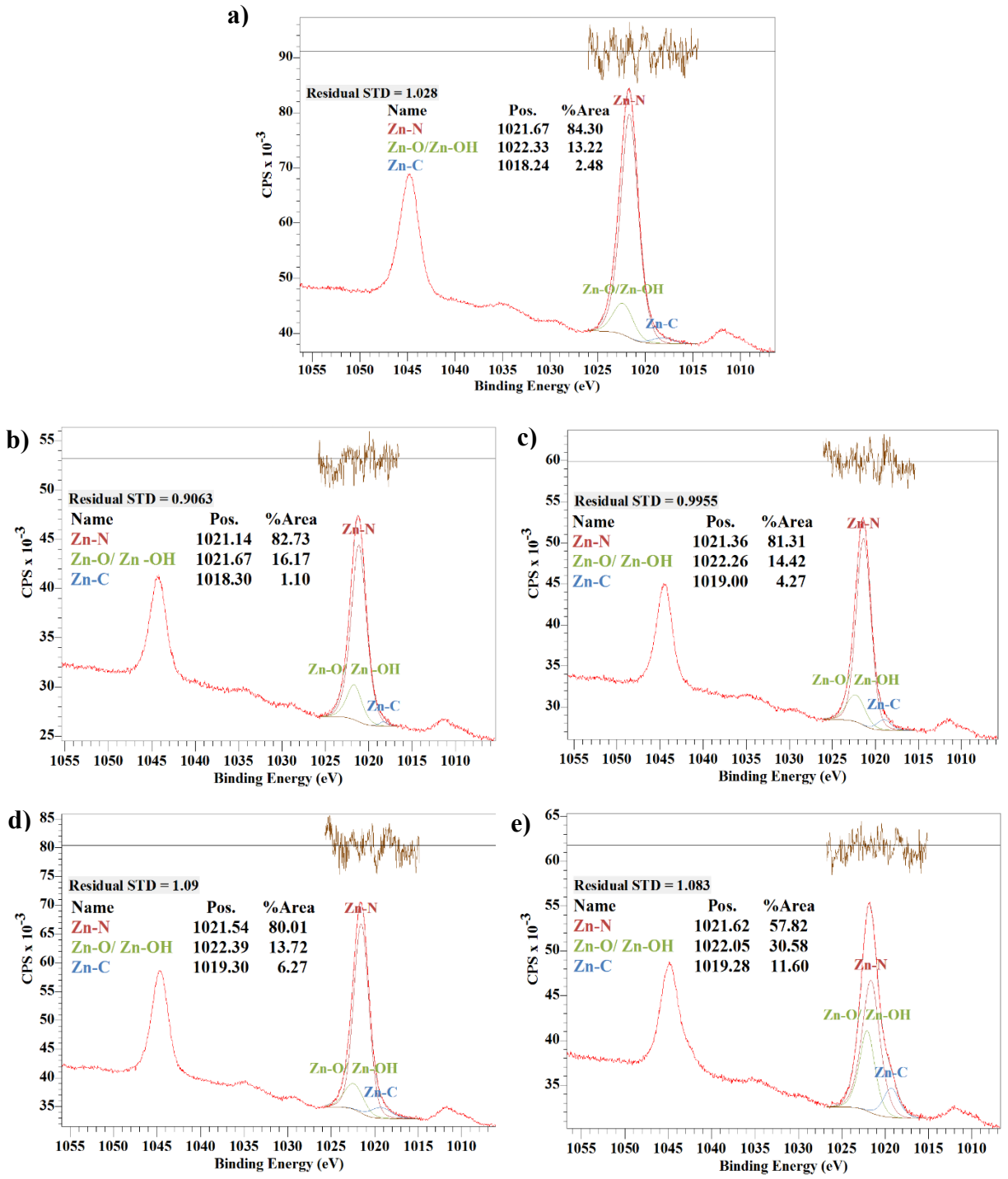

Figure 4: XPS Zn 2p narrow scan spectra of (a) ZIF-8; (b) DI water treated ZIF-8; (c-e) 0.01 M, 0.1 M, and 1 M H_2O_2 treated ZIF-8. The Data obtained from UHV-XPS experiments.

0.01 M and 0.1 M H_2O_2-treated ZIF-8. And the Zn-O/Zn-OH and Zn-C bonds appeared almost the same from pure ZIF-8 to 0.1 M H_2O_2-treated ZIF-8 samples. However, a sharp drop in the Zn-N bond and an increase in the Zn-O/Zn-OH and Zn-C bonds were found in the 1 M H_2O_2-treated ZIF-8 sample. The observation of the Zn-N and Zn-C bonds at this condition corroborates the analysis of the N-Zn and C-Zn bonds from N 1s and C 1s spectra. The rapid increase in the Zn-O/Zn-OH bond at this condition follows the ZIF-8 hydrolysis mechanisms previously proposed [41]. Nonetheless, comparing the change in the zinc bonds it may be postulated that the water did not cause a drastic change in the ZIF-8 structure, however, the oxidative species from H_2O_2 noticeably affected the ZIF-8 structure when its concentration reached 1 M.

3.3 Functional group changes:

FTIR spectroscopy was employed to analyze ZIF-8 samples and discern alterations in chemical functional groups resulting from DI water and H_2O_2 treatments. Figure 5 provides a comparison of FTIR spectra for the samples, starting with pure ZIF-8 at the top, followed by the DI water-treated sample, and subsequently the H_2O_2-treated ZIF-8 samples.

In the FTIR spectra of pure ZIF-8, the peak around 3135 cm^{-1} and 2930 cm^{-1} corresponds to the stretching vibrational mode of C-H bonds of the methyl group (-CH_3) of the imidazole linker and the entire imidazole ring. The peak around 2145 cm^{-1} corresponds to the -N=C=N- bonds of the imidazole ring. The peak around 1584 cm^{-1} corresponds to the C=C and/or C-N bonds. The peaks around 1427-1460 cm^{-1} also correspond to the entire imidazole ring. The peak at 1384 cm^{-1} corresponds to the C-C bonds which is most likely the bond between the pentagonal ring and methyl group of the imidazole ring.

Evidently, the FTIR spectra exhibit only subtle changes between the pure ZIF-8 sample, DI water-treated sample, and the samples treated with 0.01 M and 0.1 M H_2O_2. Despite the XPS analysis suggesting a gradual decrease in C-C bonds in these samples, the FTIR spectra still clearly display peaks corresponding to C-C bonds (at ~ 1384 cm^{-1}) in these samples. This observation implies that, although C-C bonds may have experienced some breakage by the effect of 0.01 M, and 0.1 M H_2O_2 treatments, they remained intact in enough quantity to show their characters peak in FTIR spectra. Notably, for the 1 M H_2O_2-treated sample, this peak was reduced, indicating a significant alteration in C-C bonds and the chemical structures surrounding them.

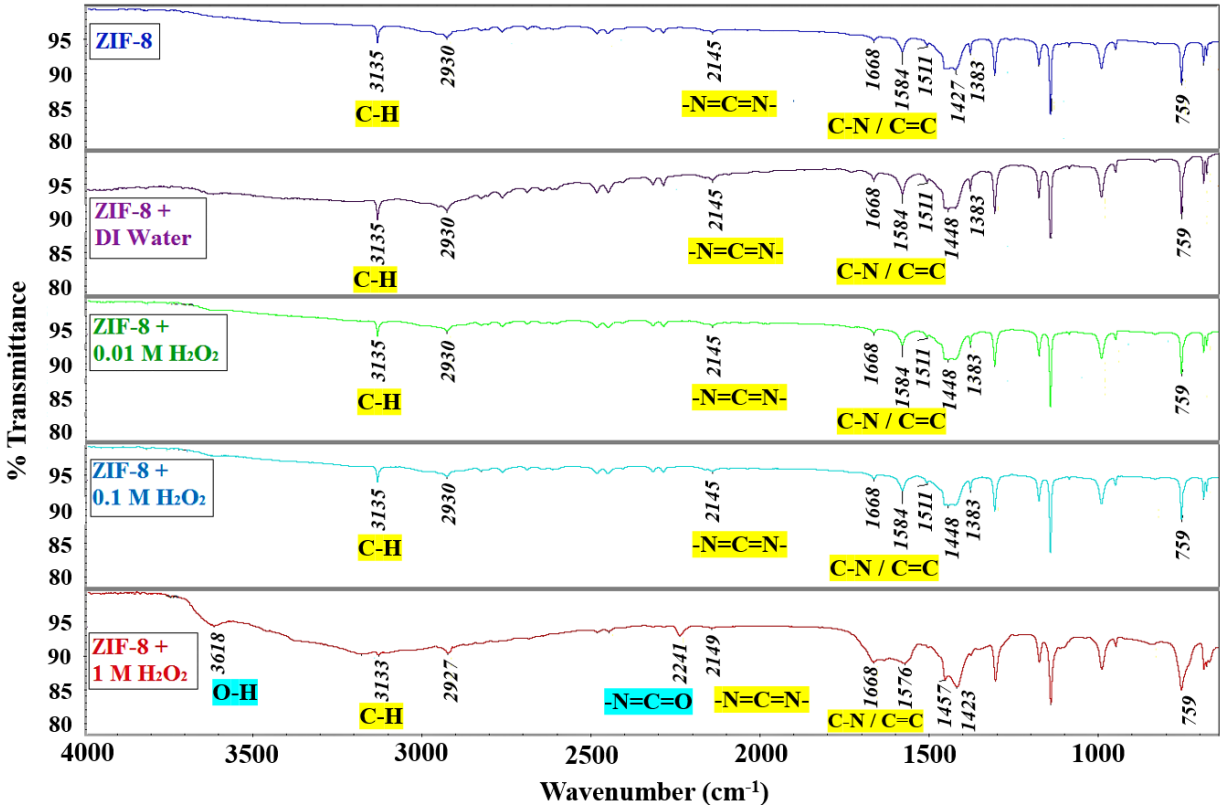

Figure 5: FTIR spectra comparison of pure ZIF-8 (top), DI water-treated ZIF-8, 0.01 M, 0.1 M, and 1 M (bottom) H_2O_2 treated ZIF-8.

Upon comparing the FTIR spectra of pure ZIF-8 and the 1 M H_2O_2-treated sample, various changes are evident in terms of different peak intensities, and the emergence of new peaks indicates the chemical changes resulting from the H_2O_2 treatment

In the FTIR spectra of 1 M H_2O_2-treated samples, a distinct peak appears at 3618 cm^{-1}, characteristic of the -OH functional group. This peak is notably more intense compared to the other treated samples. This finding aligns with the XPS analysis presented earlier. Additionally, a significant decrease in the intensity of the C-H peak around 3135 cm^{-1} is observed in the 1 M H_2O_2-treated sample compared to the other samples, implying a potential dissociation of the methyl (-CH_3) group from the imidazole ring. Furthermore, the reduction in peak intensity around 1384 cm^{-1} (corresponding to C-C bonds) also suggest a potential dissociation of -CH_3 from the imidazole ring by the 1 M H_2O_2 treatment.

The peak at 2145 cm^{-1} (-N=C=N-) notably diminishes in the 1 M H_2O_2-treated sample in comparison to the other samples. Simultaneously, a new peak emerges around 2241 cm^{-1}, corresponding to the -N=C=O bond. These two alterations, along with the seemingly unchanged peak around 1584 cm^{-1} (C=C/C-N) in comparison to other samples, indicate a potential breakdown of the imidazole ring, which could also lead to the breakdown of N-Zn bonds. The broadening of peaks in the ranges 1576-1668 cm^{-1} and 1423-1460 cm^{-1} additionally suggests structural deformation of the imidazole ring due to the effect of 1 M H_2O_2.

In summarizing the FTIR analysis of the ZIF-8 samples, no significant chemical structural changes were observed among the pure, DI water-treated, 0.01 M H_2O_2-treated, and 0.1 M H_2O_2-treated ZIF-8 samples. However, notable chemical structural changes are evident in the 1 M H_2O_2-treated ZIF-8 samples compared to the others. These changes include the presence of the -

OH group, potential dissociation of the -CH_3 group from the imidazole linker, deformation of the imidazole ring, and potential dissociation of the N-Zn bond. These observed changes in the FTIR spectra are consistent with the findings from the XPS analysis in the preceding section. Nevertheless, in various instances, literature has indicated that the ZIF-8 structure may be susceptible to water exposure [41]. While the hydrolysis process of ZIF-8 is not fully understood, the root of its structural instability in aqueous environments can be traced back to the choice of the Zinc salt used in ZIF-8 synthesis and the type of functional groups attached to the imidazole ring of the material [39, 47]. In light of existing literature and our current experimental observations, it may be hypothesized that the presence of preexisting hydroxyl (-OH) groups in synthesized ZIF-8, potentially rendering the material somewhat hydrophilic, could be a crucial factor contributing to ZIF-8's structural instability in water-based environments. However, further investigations are necessary to comprehend such processes, which fall beyond the scope of this study.

3.4 Crystal structural changes:

The changes in the crystal structure of the pure, water-treated, and H_2O_2-treated ZIF-8 samples were observed by taking the XRD patterns of the samples. The XRD patterns of each of the samples are normalized by the highest peak intensity for comparison shown in figure 6. In the XRD pattern of pure ZIF-8 sample, the prominent peaks are found at 7.3°, 10.4°, 12.7°, 14.7, 16.2, 18.1°, 26.7° which corresponds to the (011), (002), (112), (022), (013), (222), and (134) planes [5,55,56]. These diffraction peaks represent the sodalite structure's lattice planes; the XRD pattern confirms the structural purity and high crystallinity of the ZIF-8 sample.

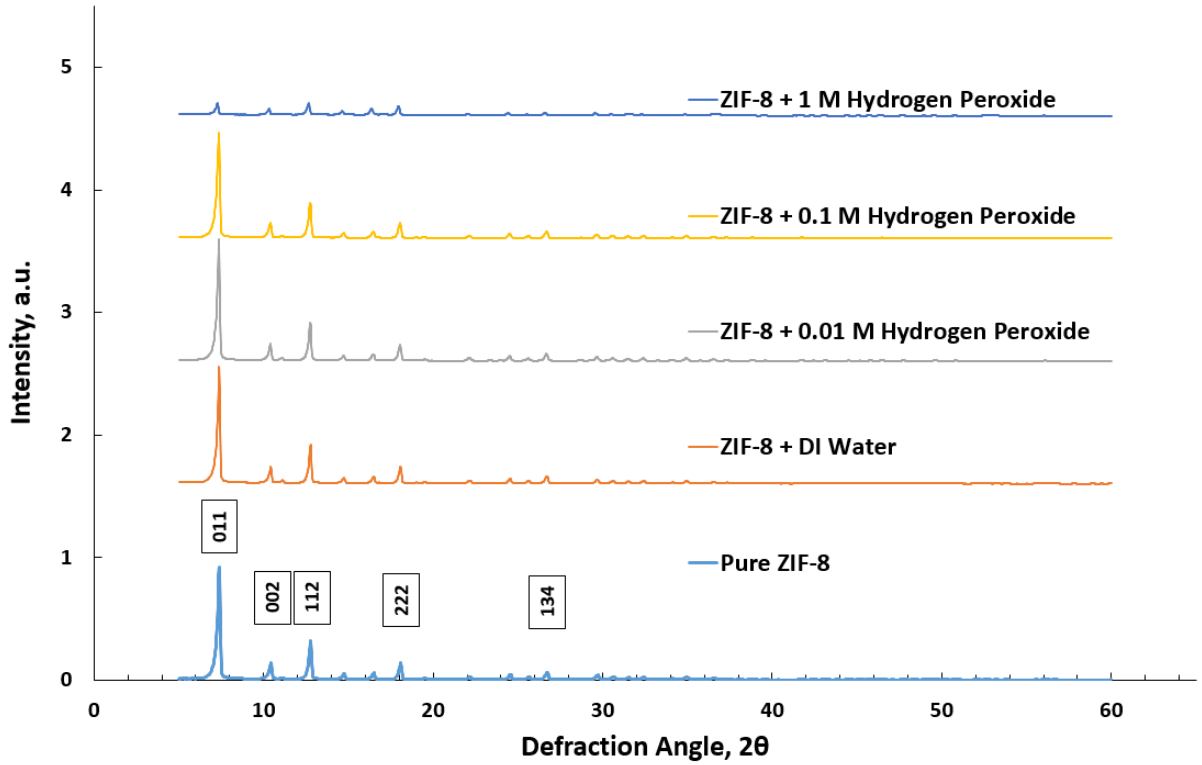

Figure 6: XRD patterns comparison of ZIF-8, DI water treated ZIF-8, 0.01 M, 0.1 M, and 1 M H_2O_2 treated ZIF-8.

The XRD pattern of the water-treated ZIF-8 sample appeared almost identical to the pure ZIF-8 one indicating that the water treatment for two hours did not alter the crystal structure of the material significantly. The XPS patterns of 0.01 M and 0.1 M H_2O_2-treated ZIF-8 sample also appeared identical with slightly increased intensity. This can be correlated with the observation of the changes in the elemental composition (table 1 and table 2), where it was seen that oxygen contents were reduced by 0.01 M and 0.1 M H_2O_2; the removal of oxygen content from ZIF-8 structure improved the degree of structural order/crystallinity of the material.

The XRD pattern of the 1 M H_2O_2-tread ZIF-8 sample shows a reduction in different peaks' intensities. Especially the peaks at 7.3° (011), 12.7° (112), and 18.1° (222) which correspond to the most exposed crystal planes of ZIF-8 are deformed significantly.

3.4 Morphological changes:

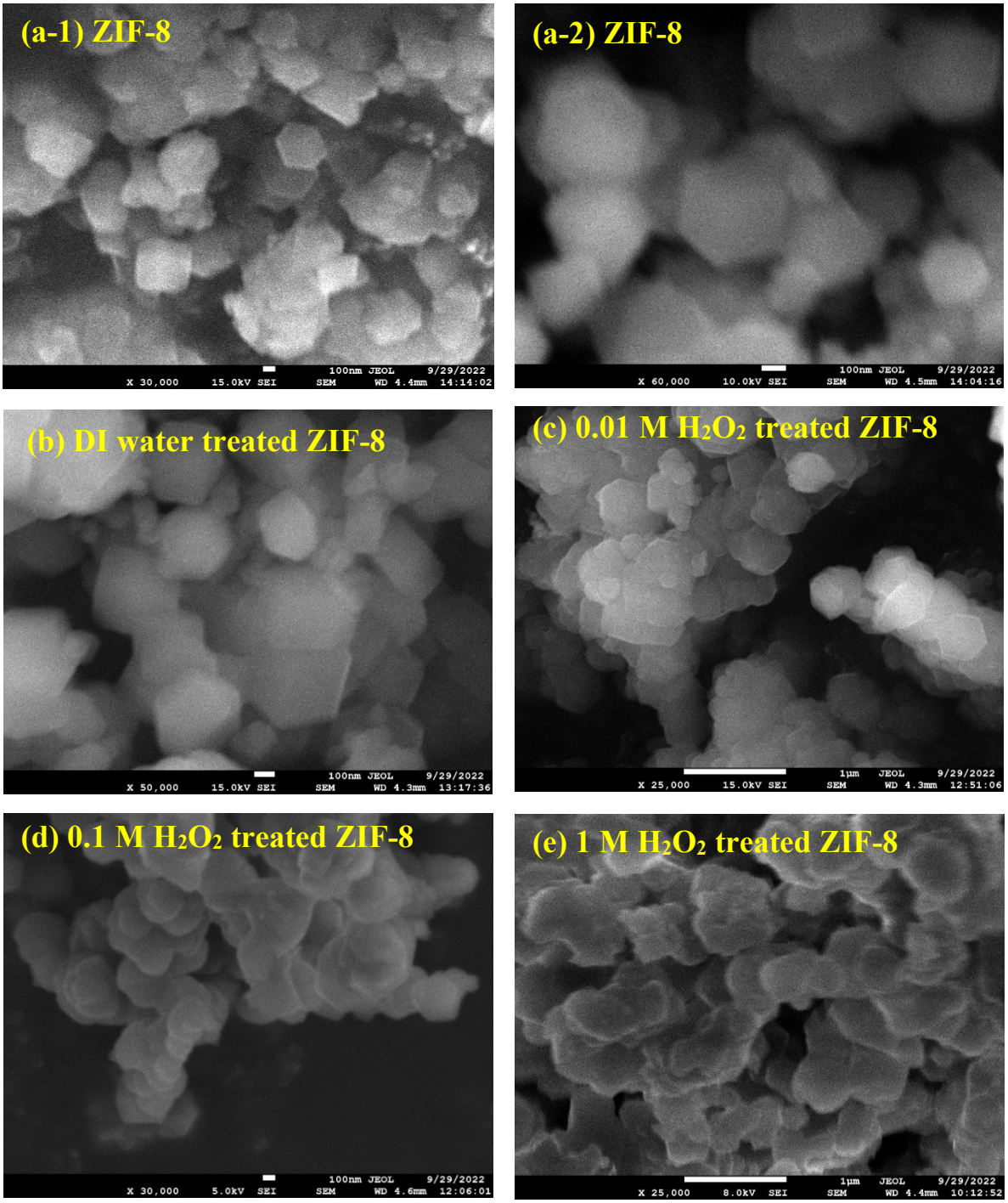

Figure 7: Morphology of (a1, a2) ZIF-8, (b) DI water treated ZIF-8; (c-e) 0.01 M, 0.1 M, and 1 M H_2O_2 treated ZIF-8 from the SEM images.

Material structural or morphological changes that occurred in ZIF-8 samples due to the water and H_2O_2 treatments were realized by comparing their SEM images in figure 7. Figure 7 (a and b) shows the morphological structure of pure ZIF-8 on a submicron scale. The well-defined crystal supper cells are observed with approximate diameters around 150 – 400 nm. These cells are composed of ZIF-8 unit-cells with porous frameworks as shown in figure 1. Figure 7 (b) shows the structure of water treated ZIF-8 sample. The crystal cells of ZIF-8 are still in a well-defined form which indicates that the DI water at room temperature did not cause significant changes in the ZIF-8 structure. Figure 7 (c) shows the submicron structure of 0.01 M H_2O_2-treated ZIF-8.

While the crystal units are visible some deformations in the shape of the crystal units are noticed. This indicates that the oxidative species from the H_2O_2 affected the chemical structure of ZIF-8. Figure 7 (d) shows the morphology of the 0.1 M H_2O_2-treated ZIF-8 sample. The degree of structural deformation is much high in this sample compared to the previous one. It appears that the crystal units are infused among each other to some degree and the shape edges of the cells became smoother. The material structure of the 1 M H_2O_2-treated ZIF-8 sample is presented in Figure 7 (e). The crystal unit ZIF-8 is almost totally altered in this condition. It can be inferred that the oxidative species from H_2O_2 at this high concentration broke the chemical bonds of the ZIF-8 structure to a high degree so that the pure structural form could not be retained. Additional images are provided in the supplementary file (Figure S-6).

4. Conclusion:

In this investigation into the structural stability of ZIF-8 when exposed to oxidative species in an aqueous environment, pure ZIF-8 samples underwent treatment with DI water and aqueous solutions containing three distinct concentrations of H_2O_2. All ZIF-8 samples, both untreated and treated, were subjected to analysis to discern alterations in elemental compositions, chemical bonds of major elements, functional groups, crystal structures, and morphology. The findings indicated that the ZIF-8 structure remained largely unchanged when in contact with water for two hours. Treatment with 0.01 M and 0.1 M H_2O_2 resulted in a marginally purer composition and crystal structure. However, the most significant physical and chemical changes in ZIF-8 were observed following treatment with 1 M H_2O_2. According to the XPS data, the treatment resulted in the breakdown of Zn-N bonds and the formation of Zn-O/Zn-OH. The 1 M H_2O_2 treatment led to a reduction in C-C bonds and an increase in C-O bonds, suggesting the elimination of the methyl group ($-CH_3$) from the ZIF-8 chemical structure by oxygen-containing groups. The FTIR spectra reveal a notable increase in the -OH functional group and a likely dissociation of $-CH_3$ groups in the 1 M H_2O_2-treated sample when compared to both the pure and water-treated ZIF-8 samples. Additionally, the XRD data indicate that H_2O_2 at a concentration of 1 M significantly affects four predominantly exposed lattice planes. These crystal structural changes are also reflected in the morphological alterations observed in the SEM images of the material. While the experimental evidence in this study offers valuable insights into understanding the structural stability of ZIF-8 in aqueous environments, these findings are expected to inform and guide future research endeavors exploring the diverse applications of ZIF-8.

Acknowledgements:

The authors acknowledge the research support from the Advanced Energy System and Microdevices (AESM) Laboratory at the New Jersey Institute of Technology (NJIT). This research used UHV-XPS, FTIR Spectrometer, and JEOL JSM-7600F SEM/EDX systems of Center for Functional Nanomaterials (CFN), which is a U.S. Department of Energy Office of Science User Facility, at Brookhaven National Laboratory under Contract No. DE-SC0012704. Authors also the acknowledge the support from the Materials Characterization Laboratory at Otto H. York Center for Environmental Engineering and Science (YCEES) at New Jersey Institute of Technology where part of the experiments were conducted.

References:

[1] J.L.C. Rowsell, O.M. Yaghi, Metal–organic frameworks: a new class of porous materials, Microporous and Mesoporous Materials. 73 (2004) 3–14. https://doi.org/https://doi.org/10.1016/j.micromeso.2004.03.034.

[2] N.L. Rosi, M. Eddaoudi, J. Kim, M. O'Keeffe, O.M. Yaghi, Advances in the chemistry of metal–organic frameworks, CrystEngComm. 4 (2002) 401–404. https://doi.org/10.1039/B203193K.

[3] J.J. Low, A.I. Benin, P. Jakubczak, J.F. Abrahamian, S.A. Faheem, R.R. Willis, Virtual High Throughput Screening Confirmed Experimentally: Porous Coordination Polymer Hydration, J Am Chem Soc. 131 (2009) 15834–15842. https://doi.org/10.1021/ja9061344.

[4] R.J. Kuppler, D.J. Timmons, Q.-R. Fang, J.-R. Li, T.A. Makal, M.D. Young, D. Yuan, D. Zhao, W. Zhuang, H.-C. Zhou, Potential applications of metal-organic frameworks, Coord Chem Rev. 253 (2009) 3042–3066. https://doi.org/https://doi.org/10.1016/j.ccr.2009.05.019.

[5] D. Saliba, M. Ammar, M. Rammal, M. Al-Ghoul, M. Hmadeh, Crystal Growth of ZIF-8, ZIF-67, and Their Mixed-Metal Derivatives, J Am Chem Soc. 140 (2018) 1812–1823. https://doi.org/10.1021/jacs.7b11589.

[6] R. Banerjee, A. Phan, B. Wang, C. Knobler, H. Furukawa, M. O'Keeffe, O.M. Yaghi, High-Throughput Synthesis of Zeolitic Imidazolate Frameworks and Application to CO_2 Capture, Science (1979). 319 (2008) 939–943. https://doi.org/10.1126/science.1152516.

[7] J.-B. Lin, T.T.T. Nguyen, R. Vaidhyanathan, J. Burner, J.M. Taylor, H. Durekova, F. Akhtar, R.K. Mah, O. Ghaffari-Nik, S. Marx, N. Fylstra, S.S. Iremonger, K.W. Dawson, P. Sarkar, P. Hovington, A. Rajendran, T.K. Woo, G.K.H. Shimizu, A scalable metal-organic framework as a durable physisorbent for carbon dioxide capture, Science (1979). 374 (2021) 1464–1469. https://doi.org/10.1126/science.abi7281.

[8] H. Demir, G.O. Aksu, H.C. Gulbalkan, S. Keskin, MOF Membranes for CO2 Capture: Past, Present and Future, Carbon Capture Science & Technology. 2 (2022) 100026. https://doi.org/https://doi.org/10.1016/j.ccst.2021.100026.

[9] N.L. Rosi, J. Eckert, M. Eddaoudi, D.T. Vodak, J. Kim, M. O'Keeffe, O.M. Yaghi, Hydrogen Storage in Microporous Metal-Organic Frameworks, Science (1979). 300 (2003) 1127–1129. https://doi.org/10.1126/science.1083440.

[10] J.L.C. Rowsell, O.M. Yaghi, Strategies for Hydrogen Storage in Metal–Organic Frameworks, Angewandte Chemie International Edition. 44 (2005) 4670–4679. https://doi.org/https://doi.org/10.1002/anie.200462786.

[11] J.L.C. Rowsell, A.R. Millward, K.S. Park, O.M. Yaghi, Hydrogen Sorption in Functionalized Metal−Organic Frameworks, J Am Chem Soc. 126 (2004) 5666–5667. https://doi.org/10.1021/ja049408c.

[12] M. Kondo, T. Yoshitomi, H. Matsuzaka, S. Kitagawa, K. Seki, Three-Dimensional Framework with Channeling Cavities for Small Molecules: [M2(4, 4′-bpy)3(NO3)4]·xH2On (M □ Co, Ni, Zn), Angewandte Chemie International Edition in English. 36 (1997) 1725–1727. https://doi.org/https://doi.org/10.1002/anie.199717251.

[13] S. Ma, D. Sun, J.M. Simmons, C.D. Collier, D. Yuan, H.-C. Zhou, Metal-Organic Framework from an Anthracene Derivative Containing Nanoscopic Cages Exhibiting High Methane Uptake, J Am Chem Soc. 130 (2008) 1012–1016. https://doi.org/10.1021/ja0771639.

[14] J.-Q. Jiang, C.-X. Yang, X.-P. Yan, Zeolitic Imidazolate Framework-8 for Fast Adsorption and Removal of Benzotriazoles from Aqueous Solution, ACS Appl Mater Interfaces. 5 (2013) 9837–9842. https://doi.org/10.1021/am403079n.

[15] J. Li, Y. Wu, Z. Li, B. Zhang, M. Zhu, X. Hu, Y. Zhang, F. Li, Zeolitic Imidazolate Framework-8 with High Efficiency in Trace Arsenate Adsorption and Removal from Water, The Journal of Physical Chemistry C. 118 (2014) 27382–27387. https://doi.org/10.1021/jp508381m.

[16] R.-Q. Zou, H. Sakurai, Q. Xu, Preparation, Adsorption Properties, and Catalytic Activity of 3D Porous Metal–Organic Frameworks Composed of Cubic Building Blocks and Alkali-Metal Ions, Angewandte Chemie International Edition. 45 (2006) 2542–2546. https://doi.org/https://doi.org/10.1002/anie.200503923.

[17] F. Gándara, B. Gomez-Lor, E. Gutiérrez-Puebla, M. Iglesias, M.A. Monge, D.M. Proserpio, N. Snejko, An Indium Layered MOF as Recyclable Lewis Acid Catalyst, Chemistry of Materials. 20 (2008) 72–76. https://doi.org/10.1021/cm071079a.

[18] S. Zhuang, B.B. Nunna, E.S. Lee, Metal organic framework-modified nitrogen-doped graphene oxygen reduction reaction catalyst synthesized by nanoscale high-energy wet ball-milling structural and electrochemical characterization, MRS Commun. 8 (2018) 40–48.

[19] S. Zhuang, H. Singh, B.B. Nunna, D. Mandal, J.A. Boscoboinik, E.S. Lee, Nitrogen-doped graphene-based catalyst with metal-reduced organic framework: Chemical analysis and structure control, Carbon N Y. 139 (2018) 933–944.

[20] W. Fujita, K. Awaga, Ferromagnetic Coordination Polymer Composed of Heterocyclic Thiazyl Radical, 1,3,5-Trithia-2,4,6-triazapentalenyl (TTTA), and Bis(hexafluoroacetylacetonato)copper(II) (Cu(hfac)2), J Am Chem Soc. 123 (2001) 3601–3602. https://doi.org/10.1021/ja002873z.

[21] C. Biswas, P. Mukherjee, M.G.B. Drew, C.J. Gómez-García, J.M. Clemente-Juan, A. Ghosh, Anion-Directed Synthesis of Metal−Organic Frameworks Based on 2-Picolinate Cu(II) Complexes: A Ferromagnetic Alternating Chain and Two Unprecedented

Ferromagnetic Fish Backbone Chains, Inorg Chem. 46 (2007) 10771–10780. https://doi.org/10.1021/ic701440x.

[22] J. Zhang, Y. Tan, W.-J. Song, Zeolitic imidazolate frameworks for use in electrochemical and optical chemical sensing and biosensing: a review, Microchimica Acta. 187 (2020) 234. https://doi.org/10.1007/s00604-020-4173-3.

[23] L. He, M. Shang, Z. Chen, Z. Yang, Metal-Organic Frameworks Nanocarriers for Functional Nucleic Acid Delivery in Biomedical Applications, The Chemical Record. n/a (n.d.) e202300018. https://doi.org/https://doi.org/10.1002/tcr.202300018.

[24] H. Niu, H. Bu, J. Zhao, Y. Zhu, Metal–Organic Frameworks-Based Nanoplatforms for the Theranostic Applications of Neurological Diseases, Small. n/a (n.d.) 2206575. https://doi.org/https://doi.org/10.1002/smll.202206575.

[25] S.A. Ahmed, D. Bagchi, H.A. Katouah, Md.N. Hasan, H.M. Altass, S.K. Pal, Enhanced Water Stability and Photoresponsivity in Metal-Organic Framework (MOF): A Potential Tool to Combat Drug-resistant Bacteria, Sci Rep. 9 (2019) 19372. https://doi.org/10.1038/s41598-019-55542-8.

[26] M. Taheri, D. Ashok, T. Sen, T.G. Enge, N.K. Verma, A. Tricoli, A. Lowe, D. R. Nisbet, T. Tsuzuki, Stability of ZIF-8 nanopowders in bacterial culture media and its implication for antibacterial properties, Chemical Engineering Journal. 413 (2021) 127511. https://doi.org/https://doi.org/10.1016/j.cej.2020.127511.

[27] O. Karagiaridi, M.B. Lalonde, W. Bury, A.A. Sarjeant, O.K. Farha, J.T. Hupp, Opening ZIF-8: A Catalytically Active Zeolitic Imidazolate Framework of Sodalite Topology with

Unsubstituted Linkers, J Am Chem Soc. 134 (2012) 18790–18796. https://doi.org/10.1021/ja308786r.

[28] S.R. Venna, M.A. Carreon, Highly Permeable Zeolite Imidazolate Framework-8 Membranes for CO2/CH4 Separation, J Am Chem Soc. 132 (2010) 76–78. https://doi.org/10.1021/ja909263x.

[29] Y.W. Abraha, C.-W. Tsai, J.W.H. Niemantsverdriet, E.H.G. Langner, Optimized CO2 Capture of the Zeolitic Imidazolate Framework ZIF-8 Modified by Solvent-Assisted Ligand Exchange, ACS Omega. 6 (2021) 21850–21860. https://doi.org/10.1021/acsomega.1c01130.

[30] M. Zhou, Q. Wang, L. Zhang, Y.-C. Liu, Y. Kang, Adsorption Sites of Hydrogen in Zeolitic Imidazolate Frameworks, J Phys Chem B. 113 (2009) 11049–11053. https://doi.org/10.1021/jp904170s.

[31] N.R. and S.M. Lin Xiang and Champness, Hydrogen, Methane and Carbon Dioxide Adsorption in Metal-Organic Framework Materials, in: M. Schröder (Ed.), Functional Metal-Organic Frameworks: Gas Storage, Separation and Catalysis, Springer Berlin Heidelberg, Berlin, Heidelberg, 2010: pp. 35–76. https://doi.org/10.1007/128_2009_21.

[32] T.T. Isimjan, H. Kazemian, S. Rohani, A.K. Ray, Photocatalytic activities of Pt/ZIF-8 loaded highly ordered TiO2 nanotubes, J. Mater. Chem. 20 (2010) 10241–10245. https://doi.org/10.1039/C0JM02152K.

[33] X. Dai, X. Li, M. Zhang, J. Xie, X. Wang, Zeolitic Imidazole Framework/Graphene Oxide Hybrid Functionalized Poly(lactic acid) Electrospun Membranes: A Promising

Environmentally Friendly Water Treatment Material, ACS Omega. 3 (2018) 6860–6866. https://doi.org/10.1021/acsomega.8b00792.

[34] J. Wang, Y. Wang, Y. Zhang, A. Uliana, J. Zhu, J. Liu, B. der Bruggen, Zeolitic Imidazolate Framework/Graphene Oxide Hybrid Nanosheets Functionalized Thin Film Nanocomposite Membrane for Enhanced Antimicrobial Performance, ACS Appl Mater Interfaces. 8 (2016) 25508–25519. https://doi.org/10.1021/acsami.6b06992.

[35] W. Xue, Q. Zhou, F. Li, B.S. Ondon, Zeolitic imidazolate framework-8 (ZIF-8) as robust catalyst for oxygen reduction reaction in microbial fuel cells, J Power Sources. 423 (2019) 9–17. https://doi.org/https://doi.org/10.1016/j.jpowsour.2019.03.017.

[36] M. Thomas, R. Illathvalappil, S. Kurungot, B.N. Nair, A.A.P. Mohamed, G.M. Anilkumar, T. Yamaguchi, U.S. Hareesh, Graphene Oxide Sheathed ZIF-8 Microcrystals: Engineered Precursors of Nitrogen-Doped Porous Carbon for Efficient Oxygen Reduction Reaction (ORR) Electrocatalysis, ACS Appl Mater Interfaces. 8 (2016) 29373–29382. https://doi.org/10.1021/acsami.6b06979.

[37] Z. Jia, G. Wu, D. Wu, Z. Tong, W.S. Winston Ho, Preparation of ultra-stable ZIF-8 dispersions in water and ethanol, Journal of Porous Materials. 24 (2017) 1655–1660. https://doi.org/10.1007/s10934-017-0405-2.

[38] K.S. Park, Z. Ni, A.P. Côté, J.Y. Choi, R. Huang, F.J. Uribe-Romo, H.K. Chae, M. O'Keeffe, O.M. Yaghi, Exceptional chemical and thermal stability of zeolitic imidazolate frameworks, Proceedings of the National Academy of Sciences. 103 (2006) 10186–10191. https://doi.org/10.1073/pnas.0602439103.

[39] L. Sheng, F. Yang, C. Wang, J. Yu, L. Zhang, Y. Pan, Comparison of the hydrothermal stability of ZIF-8 nanocrystals and polycrystalline membranes derived from zinc salt variations, Mater Lett. 197 (2017) 184–187. https://doi.org/https://doi.org/10.1016/j.matlet.2017.03.077.

[40] M. Taheri, T. Tsuzuki, Photo-accelerated Hydrolysis of Metal Organic Framework ZIF-8, ACS Mater Lett. 3 (2021) 255–260. https://doi.org/10.1021/acsmaterialslett.0c00522.

[41] H. Zhang, M. Zhao, Y. Yang, Y.S. Lin, Hydrolysis and condensation of ZIF-8 in water, Microporous and Mesoporous Materials. 288 (2019) 109568. https://doi.org/https://doi.org/10.1016/j.micromeso.2019.109568.

[42] H. Zhang, D. Liu, Y. Yao, B. Zhang, Y.S. Lin, Stability of ZIF-8 membranes and crystalline powders in water at room temperature, J Memb Sci. 485 (2015) 103–111. https://doi.org/https://doi.org/10.1016/j.memsci.2015.03.023.

[43] H. Zhang, M. Zhao, Y.S. Lin, Stability of ZIF-8 in water under ambient conditions, Microporous and Mesoporous Materials. 279 (2019) 201–210. https://doi.org/https://doi.org/10.1016/j.micromeso.2018.12.035.

[44] S. Tanaka, Y. Tanaka, A Simple Step toward Enhancing Hydrothermal Stability of ZIF-8, ACS Omega. 4 (2019) 19905–19912. https://doi.org/10.1021/acsomega.9b02812.

[45] F. Tian, A.M. Cerro, A.M. Mosier, H.K. Wayment-Steele, R.S. Shine, A. Park, E.R. Webster, L.E. Johnson, M.S. Johal, L. Benz, Surface and Stability Characterization of a Nanoporous ZIF-8 Thin Film, The Journal of Physical Chemistry C. 118 (2014) 14449–14456. https://doi.org/10.1021/jp5041053.

[46] P.C. Metz, M.R. Ryder, A. Ganesan, S. Bhattacharyya, S.C. Purdy, S. Nair, K. Page, Structure Evolution of Chemically Degraded ZIF-8, The Journal of Physical Chemistry C. 126 (2022) 9736–9741. https://doi.org/10.1021/acs.jpcc.2c02217.

[47] A.U. Ortiz, A.P. Freitas, A. Boutin, A.H. Fuchs, F.-X. Coudert, What makes zeolitic imidazolate frameworks hydrophobic or hydrophilic? The impact of geometry and functionalization on water adsorption, Phys. Chem. Chem. Phys. 16 (2014) 9940–9949. https://doi.org/10.1039/C3CP54292K.

[48] H. Jasuja, Y. Huang, K.S. Walton, Adjusting the Stability of Metal–Organic Frameworks under Humid Conditions by Ligand Functionalization, Langmuir. 28 (2012) 16874–16880. https://doi.org/10.1021/la304151r.

[49] J. Li, S. Chen, N. Yang, M. Deng, S. Ibraheem, J. Deng, J. Li, L. Li, Z. Wei, Ultrahigh-Loading Zinc Single-Atom Catalyst for Highly Efficient Oxygen Reduction in Both Acidic and Alkaline Media, Angewandte Chemie International Edition. 58 (2019) 7035–7039. https://doi.org/https://doi.org/10.1002/anie.201902109.

[50] C. Xie, L. Lin, L. Huang, Z. Wang, Z. Jiang, Z. Zhang, B. Han, Zn-Nx sites on N-doped carbon for aerobic oxidative cleavage and esterification of C(CO)-C bonds, Nat Commun. 12 (2021) 4823. https://doi.org/10.1038/s41467-021-25118-0.

[51] C.-W. Tsai, E.H.G. Langner, R.A. Harris, Computational study of ZIF-8 analogues with electron donating and withdrawing groups for CO2 adsorption, Microporous and Mesoporous Materials. 288 (2019) 109613. https://doi.org/https://doi.org/10.1016/j.micromeso.2019.109613.

[52] P. Ying, J. Zhang, X. Zhang, Z. Zhong, Impacts of Functional Group Substitution and Pressure on the Thermal Conductivity of ZIF-8, The Journal of Physical Chemistry C. 124 (2020) 6274–6283. https://doi.org/10.1021/acs.jpcc.0c00597.

[53] K. Shen, L. Zhang, X. Chen, L. Liu, D. Zhang, Y. Han, J. Chen, J. Long, R. Luque, Y. Li, B. Chen, Ordered macro-microporous metal-organic framework single crystals, Science (1979). 359 (2018) 206–210. https://doi.org/10.1126/science.aao3403.

[54] C. Avci, J. Ariñez-Soriano, A. Carné-Sánchez, V. Guillerm, C. Carbonell, I. Imaz, D. Maspoch, Post-Synthetic Anisotropic Wet-Chemical Etching of Colloidal Sodalite ZIF Crystals, Angewandte Chemie International Edition. 54 (2015) 14417–14421. https://doi.org/https://doi.org/10.1002/anie.201507588.

Tables:

Table 1: Surface elemental composition of ZIF-8, DI water treated ZIF-8, and 0.1, 0.1, and 1 M H_2O_2 treated ZIF-8 samples; obtained by UHV-XPS survey scan.

Samples	Nitrogen (N) relative atomic ratio	Zinc (Zn) relative atomic ratio	Carbon (C) relative atomic ratio	Oxygen (O) relative atomic ratio
	(%)	(%)	(%)	(%)
ZIF-8	25.87 ± 0.85	3.45 ± 0.09	62.94 ± 1.35	7.74 ± 0.58
ZIF-8 + H_2O (Water)	24.59 ± 0.50	3.23 ± 0.19	63.69 ± 0.82	8.49 ± 0.40
ZIF-8 + 0.01 M H_2O_2	25.76 ± 0.31	3.12 ± 0.28	64.95 ± 0.85	6.17 ± 0.94
ZIF-8 + 0.1 M H_2O_2	26.64 ± 1.95	3.19 ± 0.09	64.01 ± 0.53	6.16 ± 1.96
ZIF-8 + 1 M H_2O_2	24.91 ± 0.38	2.84 ± 0.09	55.34 ± 2.27	16.91 ± 2.11

Table 3: Bulk elemental composition of ZIF-8, DI water treated ZIF-8, and 0.1, 0.1, and 1 M H_2O_2 treated ZIF-8 samples; obtained by EDX analysis.

Samples	Nitrogen (N) relative atomic ratio	Zinc (Zn) relative atomic ratio	Carbon (C) relative atomic ratio	Oxygen (O) relative atomic ratio
	(%)	(%)	(%)	(%)
ZIF-8	29.37 ± 4.06	7.51 ± 1.08	61.88 ± 3.10	1.24 ± 0.41
ZIF-8 + H_2O (Water)	27.86 ± 2.62	6.32 ± 1.24	64.54 ± 3.43	1.28 ± 0.68
ZIF-8 + 0.01 M H_2O_2	24.76 ± 1.67	10.27 ± 2.38	63.74 ± 1.06	1.40 ± 0.50
ZIF-8 + 0.1 M H_2O_2	30.87 ± 1.72	5.47 ± 0.76	62.30 ± 2.12	1.35 ± 0.48
ZIF-8 + 1 M H_2O_2	29.87 ± 0.84	7.07 ± 0.87	58.22 ± 0.37	4.85 ± 0.07

Figure Captions:

Figure 1: Schematics of ZIF-8 crystal unit cell; sodalite shape of the unit cell; formation of ZIF-8 crystal from unit cells; and ZIF-8 crystal with planes denoted with miller indices from an arbitrary reference coordinate. Schematics are not in actual size scales.

Figure 2: XPS C 1s narrow scan spectra of (a) ZIF-8; (b) DI water treated ZIF-8; (c-e) 0.01 M, 0.1 M, and 1 M H_2O_2 treated ZIF-8. The Data obtained from UHV-XPS experiments.

Figure 3: XPS N 1s narrow scan spectra of (a) ZIF-8; (b) DI water treated ZIF-8; (c-e) 0.01 M, 0.1 M, and 1 M H_2O_2 treated ZIF-8. The Data obtained from UHV-XPS experiments.

Figure 4: XPS Zn 2p narrow scan spectra of (a) ZIF-8; (b) DI water treated ZIF-8; (c-e) 0.01 M, 0.1 M and 1 M H_2O_2 treated ZIF-8. The Data obtained from UHV-XPS experiments.

Figure 8: FTIR spectra comparison of pure ZIF-8 (top), DI water-treated ZIF-8, 0.01 M, 0.1 M, and 1 M (bottom) H_2O_2 treated ZIF-8.

Figure 6: XRD patterns comparison of ZIF-8, DI water treated ZIF-8, 0.01 M, 0.1 M, and 1 M H_2O_2 treated ZIF-8.

Figure 7: Morphology of (a1, a2) ZIF-8, (b) DI water treated ZIF-8; (c-e) 0.01 M, 0.1 M, and 1 M H_2O_2 treated ZIF-8 from the SEM images.

Figures:

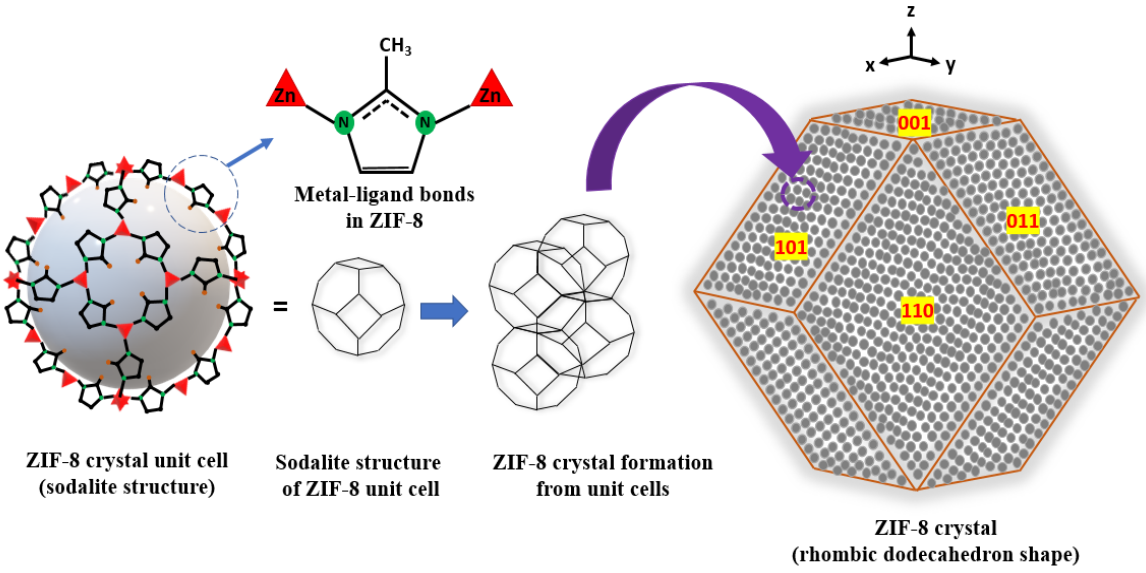
CH3
Zn
N
N
Zn
Metal-ligand bonds
in ZIF-8
=
z
x
y
001
011
101
110
ZIF-8 crystal unit cell
(sodalite structure)
Sodalite structure
of ZIF-8 unit cell
ZIF-8 crystal formation
from unit cells
ZIF-8 crystal
(rhombic dodecahedron shape)

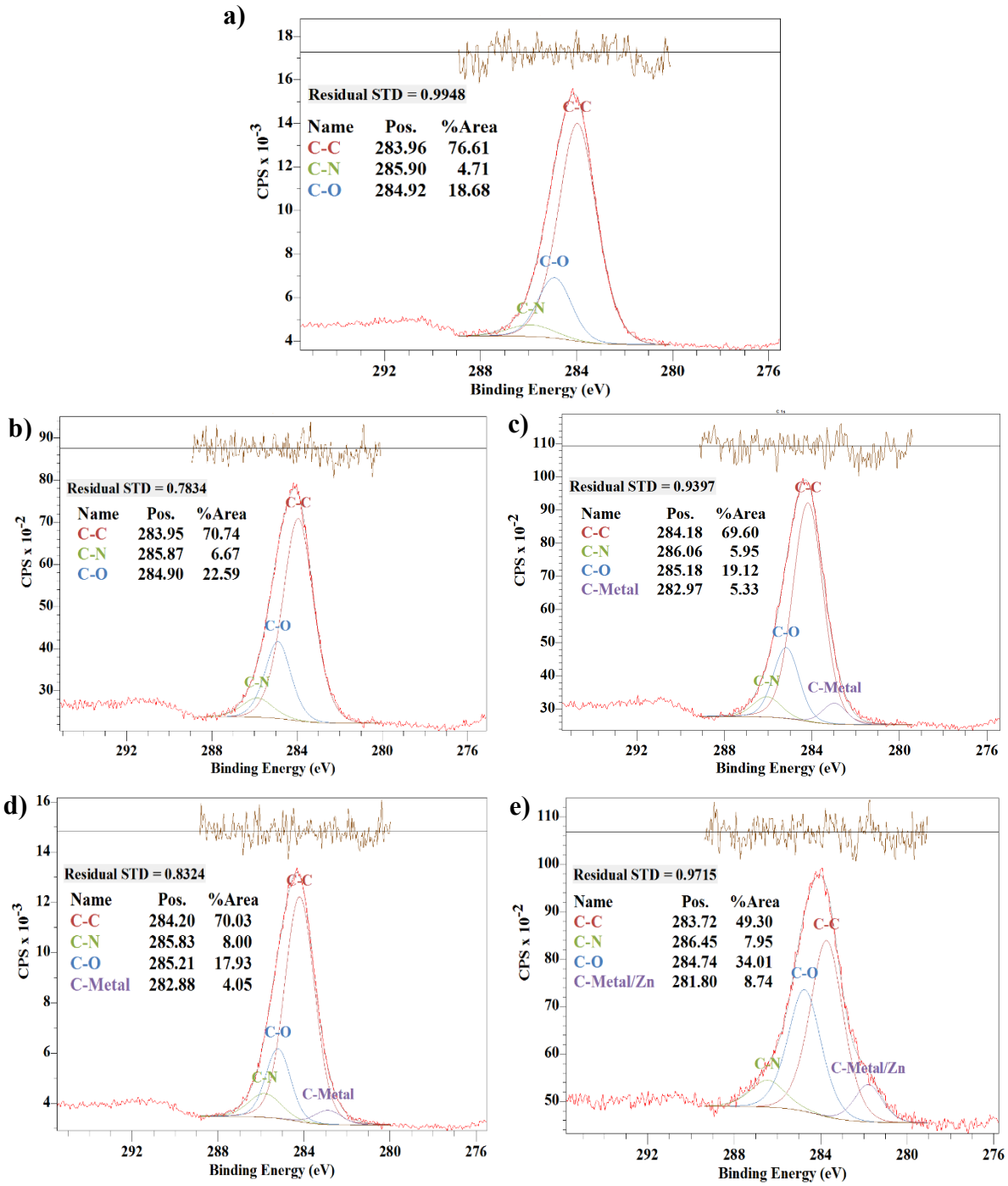
a)
Residual STD = 0.9948
Name Pos. %Area
C-C 283.96 76.61
C-N 285.90 4.71
C-O 284.92 18.68
CPS x 10-3
Binding Energy (eV)
b)
Residual STD = 0.7834
Name Pos. %Area
C-C 283.95 70.74
C-N 285.87 6.67
C-O 284.90 22.59
CPS x 10-2
Binding Energy (eV)
c)
Residual STD = 0.9397
Name Pos. %Area
C-C 284.18 69.60
C-N 286.06 5.95
C-O 285.18 19.12
C-Metal 282.97 5.33
CPS x 10-2
Binding Energy (eV)
d)
Residual STD = 0.8324
Name Pos. %Area
C-C 284.20 70.03
C-N 285.83 8.00
C-O 285.21 17.93
C-Metal 282.88 4.05
CPS x 10-3
Binding Energy (eV)
e)
Residual STD = 0.9715
Name Pos. %Area
C-C 283.72 49.30
C-N 286.45 7.95
C-O 284.74 34.01
C-Metal/Zn 281.80 8.74
CPS x 10-2
Binding Energy (eV)

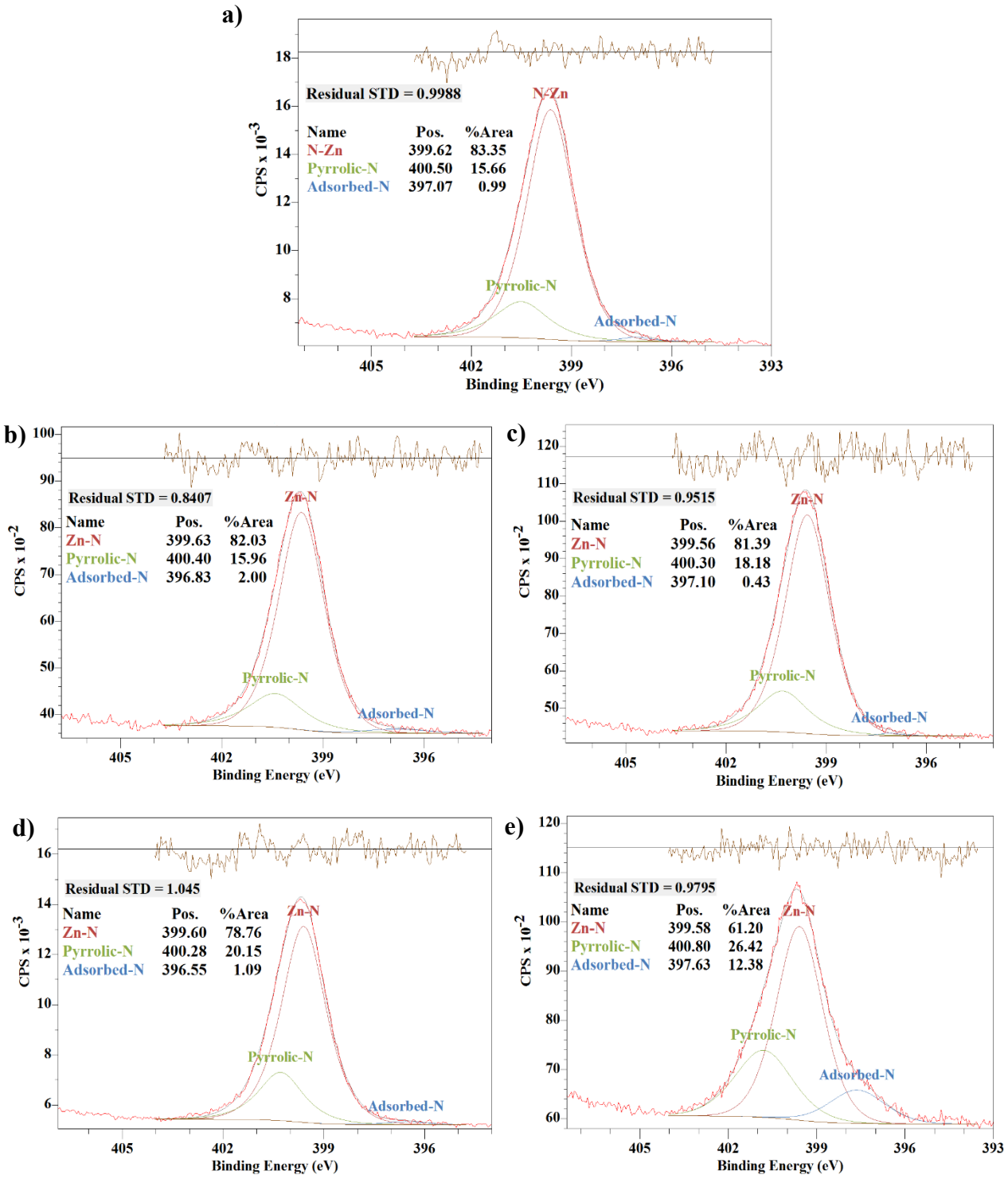
a)
Residual STD = 0.9988
Name Pos. %Area
N-Zn 399.62 83.35
Pyrrolic-N 400.50 15.66
Adsorbed-N 397.07 0.99
N-Zn
Pyrrolic-N
Adsorbed-N
CPS x 10-3
Binding Energy (eV)
b)
Residual STD = 0.8407
Name Pos. %Area
Zn-N 399.63 82.03
Pyrrolic-N 400.40 15.96
Adsorbed-N 396.83 2.00
Zn-N
Pyrrolic-N
Adsorbed-N
CPS x 10-2
Binding Energy (eV)
c)
Residual STD = 0.9515
Name Pos. %Area
Zn-N 399.56 81.39
Pyrrolic-N 400.30 18.18
Adsorbed-N 397.10 0.43
Zn-N
Pyrrolic-N
Adsorbed-N
CPS x 10-2
Binding Energy (eV)
d)
Residual STD = 1.045
Name Pos. %Area
Zn-N 399.60 78.76
Pyrrolic-N 400.28 20.15
Adsorbed-N 396.55 1.09
Zn-N
Pyrrolic-N
Adsorbed-N
CPS x 10-3
Binding Energy (eV)
e)
Residual STD = 0.9795
Name Pos. %Area
Zn-N 399.58 61.20
Pyrrolic-N 400.80 26.42
Adsorbed-N 397.63 12.38
Zn-N
Pyrrolic-N
Adsorbed-N
CPS x 10-2
Binding Energy (eV)

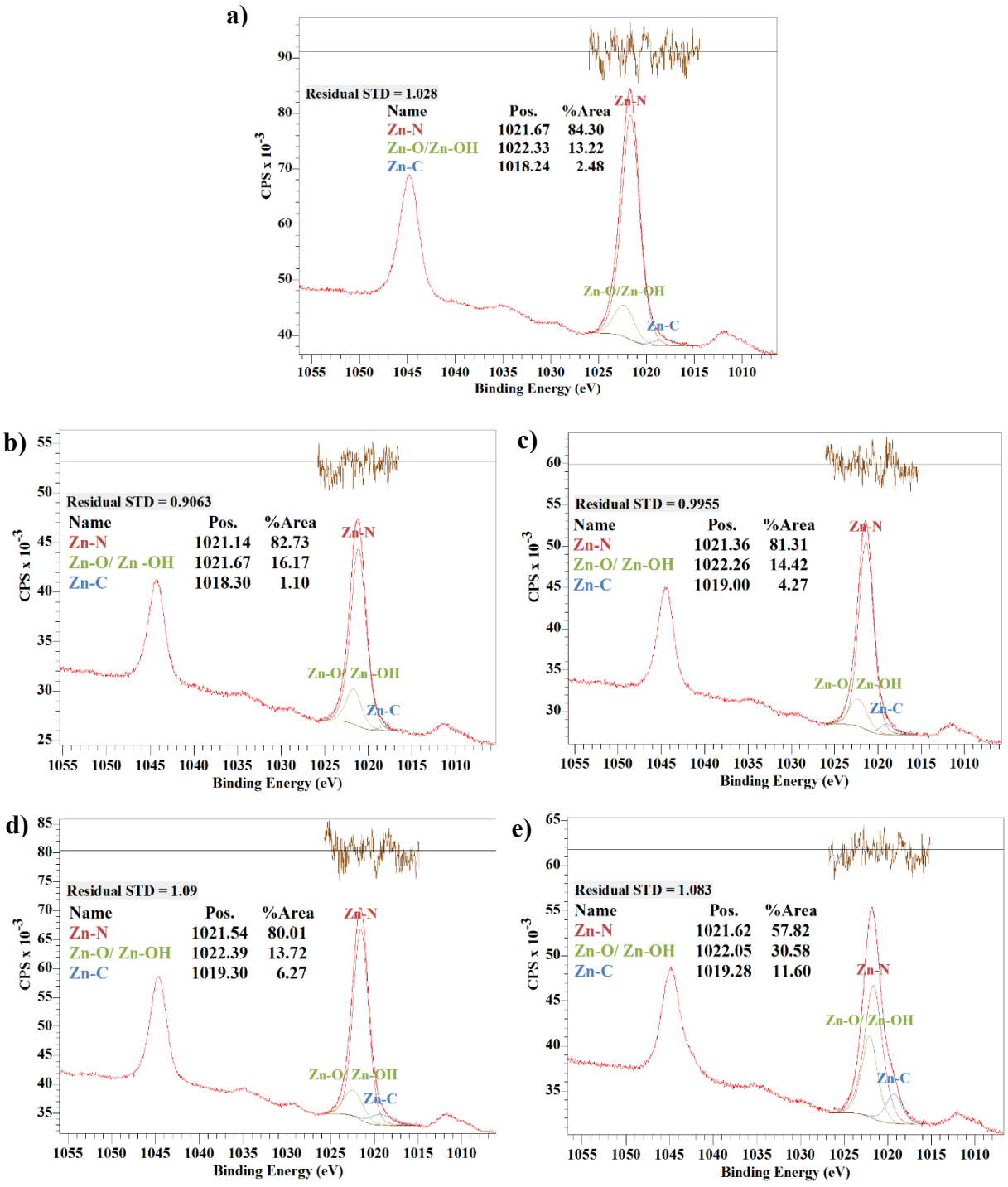
a)
Residual STD = 1.028
Name Pos. %Area
Zn-N 1021.67 84.30
Zn-O/Zn-OH 1022.33 13.22
Zn-C 1018.24 2.48
b)
Residual STD = 0.9063
Name Pos. %Area
Zn-N 1021.14 82.73
Zn-O/ Zn -OH 1021.67 16.17
Zn-C 1018.30 1.10
c)
Residual STD = 0.9955
Name Pos. %Area
Zn-N 1021.36 81.31
Zn-O/ Zn-OH 1022.26 14.42
Zn-C 1019.00 4.27
d)
Residual STD = 1.09
Name Pos. %Area
Zn-N 1021.54 80.01
Zn-O/ Zn-OH 1022.39 13.72
Zn-C 1019.30 6.27
e)
Residual STD = 1.083
Name Pos. %Area
Zn-N 1021.62 57.82
Zn-O/ Zn-OH 1022.05 30.58
Zn-C 1019.28 11.60
CPS x 10-3
Binding Energy (eV)

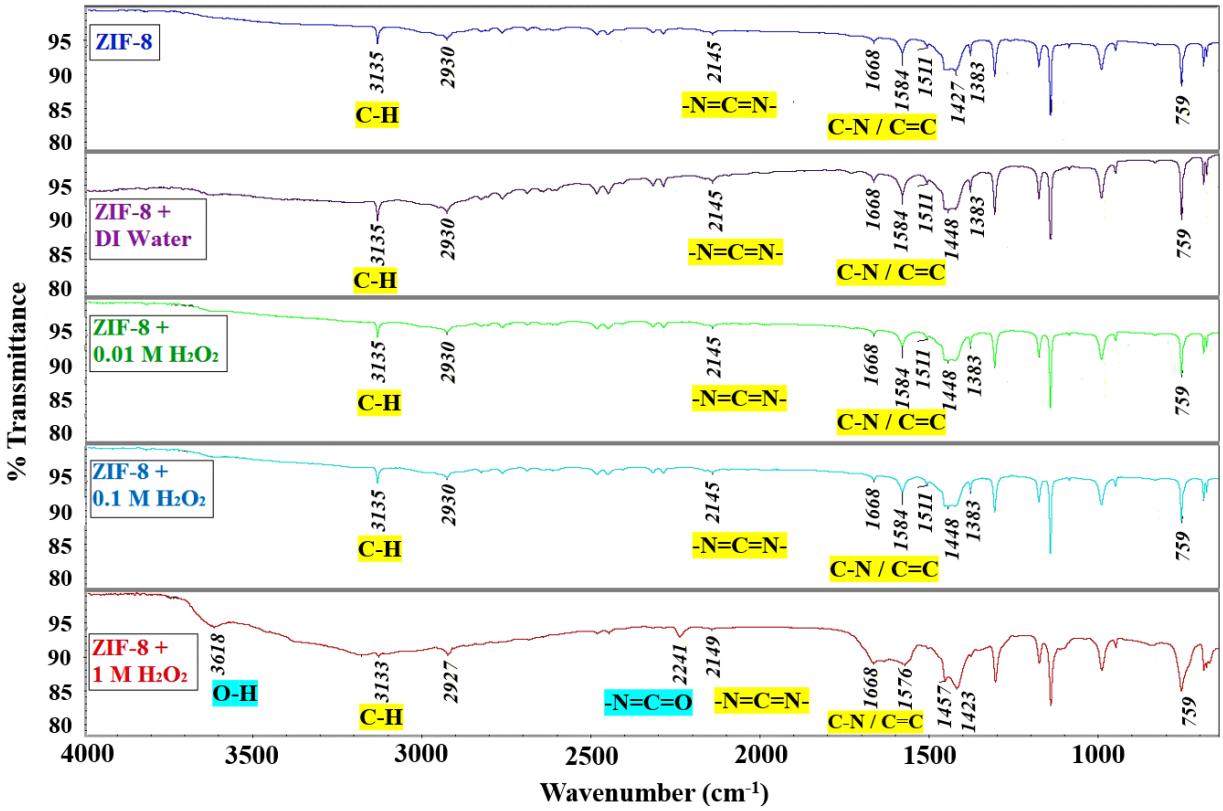
ZIF-8
3135
2930
2145
1668
1584
1511
1427
1383
759
C-H
-N=C=N-
C-N / C=C
ZIF-8 +
DI Water
3135
2930
2145
1668
1584
1511
1448
1383
759
C-H
-N=C=N-
C-N / C=C
ZIF-8 +
0.01 M H2O2
3135
2930
2145
1668
1584
1511
1448
1383
759
C-H
-N=C=N-
C-N / C=C
ZIF-8 +
0.1 M H2O2
3135
2930
2145
1668
1584
1511
1448
1383
759
C-H
-N=C=N-
C-N / C=C
ZIF-8 +
1 M H2O2
3618
3133
2927
2241
2149
1668
1576
1457
1423
759
O-H
C-H
-N=C=O
-N=C=N-
C-N / C=C
% Transmittance
95
90
85
80
4000
3500
3000
2500
2000
1500
1000
Wavenumber (cm-1)

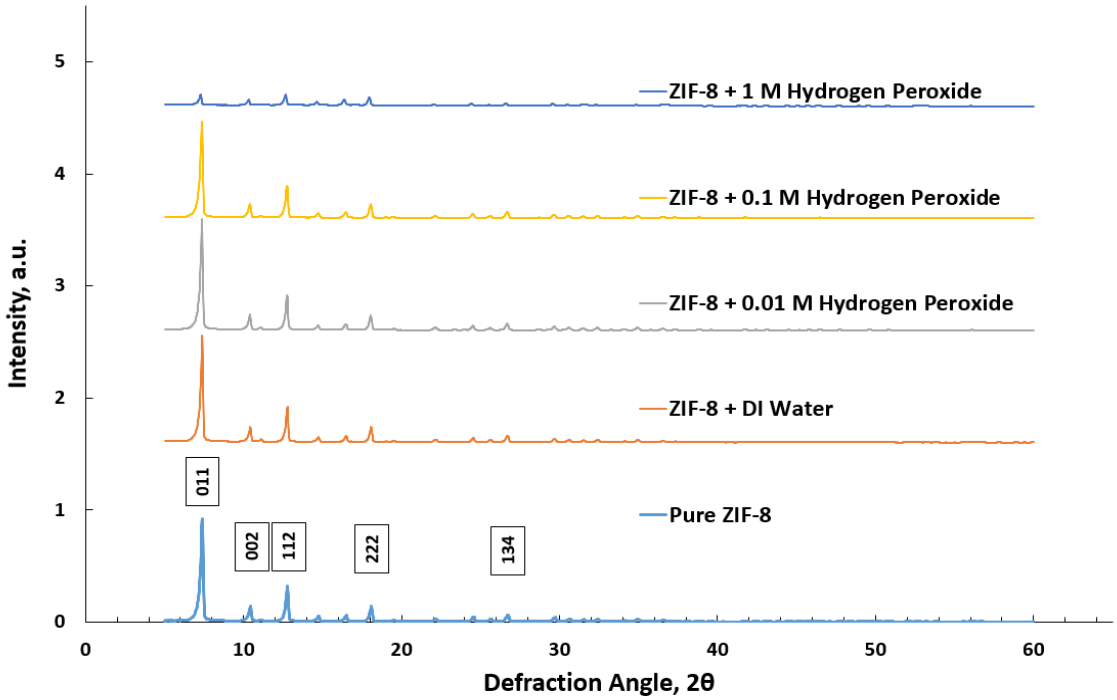
Intensity, a.u.
Defraction Angle, 2θ
ZIF-8 + 1 M Hydrogen Peroxide
ZIF-8 + 0.1 M Hydrogen Peroxide
ZIF-8 + 0.01 M Hydrogen Peroxide
ZIF-8 + DI Water
Pure ZIF-8
011
002
112
222
134
0
1
2
3
4
5
0
10
20
30
40
50
60

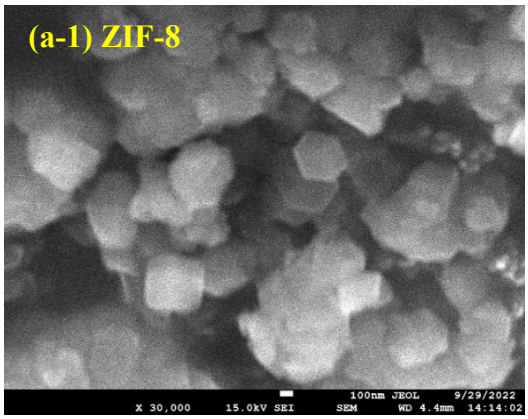
(a-1) ZIF-8
X 30,000 15.0kV SEI 100nm JEOL SEM WD 4.4mm 9/29/2022 14:14:02

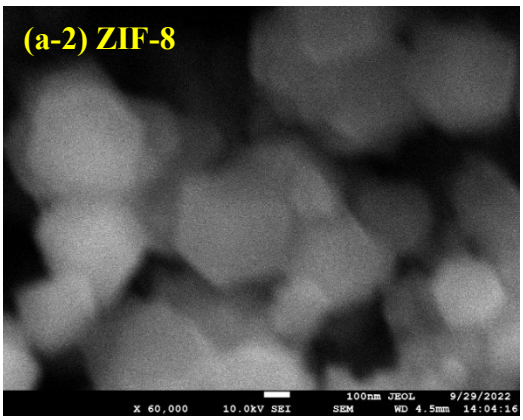
(a-2) ZIF-8
X 60,000 10.0kV SEI 100nm JEOL SEM WD 4.5mm 9/29/2022 14:04:16

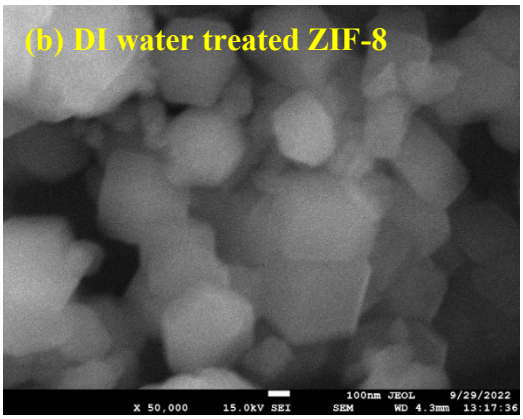
(b) DI water treated ZIF-8
X 50,000 15.0kV SEI 100nm JEOL SEM WD 4.3mm 9/29/2022 13:17:36

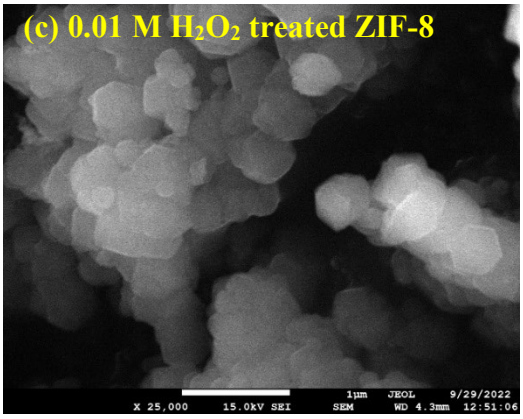
(c) 0.01 M H_2O_2 treated ZIF-8
X 25,000 15.0kV SEI 1μm JEOL SEM WD 4.3mm 9/29/2022 12:51:06

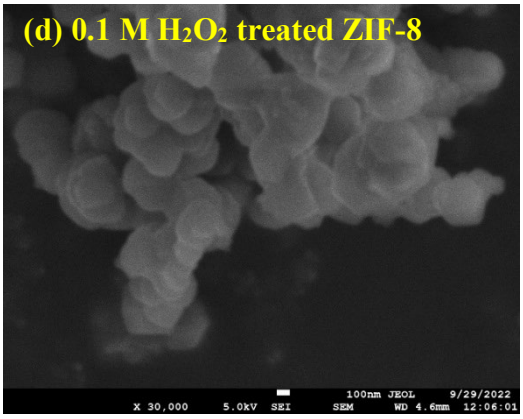
(d) 0.1 M H_2O_2 treated ZIF-8
X 30,000 5.0kV SEI 100nm JEOL SEM WD 4.6mm 9/29/2022 12:06:01

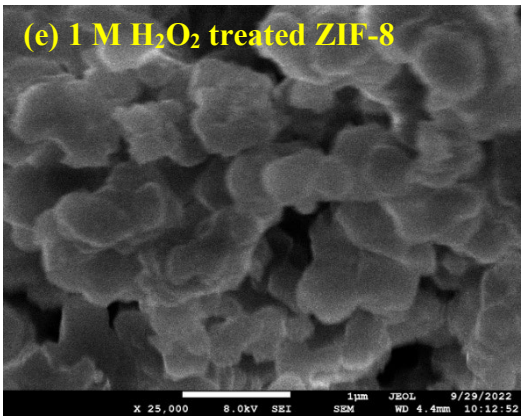
(e) 1 M H_2O_2 treated ZIF-8
X 25,000 8.0kV SEI 1μm JEOL SEM WD 4.4mm 9/29/2022 10:12:52